GEOPHYSICS

UNIVERSITY OF MISSOURI - ROLLA

TITLE

SEISMIC DETECTION OF SUBTERRANEAN CAVITIES

TYPE OF REPORT (TECHNICAL, FINAL, ETC.)

FINAL

AUTHOR (S)

RICHARD D. RECHTIEN
DAVID M. STEWART
THOM CAVANAUGH

DATE

30 NOVEMBER 1976

U. S. ARMY RESEARCH OFFICE

CONTRACT / GRANT NUMBER

DAHC 04 74 G 0004
DAAG 29 76 G 0006

INSTITUTION

UNIVERSITY OF MISSOURI
DEPARTMENT OF GEOLOGY
ROLLA, MISSOURI 65401

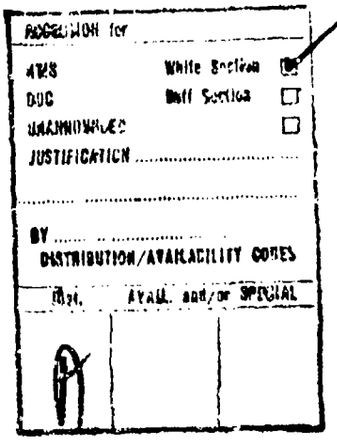

APPROVED FOR PUBLIC RELEASE; DISTRIBUTION UNLIMITED.

THE FINDINGS IN THIS REPORT ARE NOT TO BE CONSTRUED AS AN OFFICIAL DEPARTMENT OF THE ARMY POSITION, UNLESS SO DESIGNATED BY OTHER AUTHORIZED DOCUMENTS.

SEISMIC DETECTION OF SUBTERRANEAN CAVITIES

by

Richard D. Rechtien
David M. Stewart
Thom Cavanaugh

SECURITY CLASSIFICATION OF THIS PAGE (When Data Entered)

REPORT DOCUMENTATION PAGE

READ INSTRUCTIONS BEFORE COMPLETING FORM

(9) 1. REPORT NUMBER: Final Rept. Sep 73- Aug 76 | 2. GOVT ACCESSION NO. | 3. RECIPIENT'S CATALOG NUMBER

(6) 4. TITLE (and Subtitle): SEISMIC DETECTION OF SUBTERRANEAN CAVITIES,

5. TYPE OF REPORT & PERIOD COVERED: FINAL 9/73 - 8/76

6. PERFORMING ORG. REPORT NUMBER

(10) 7. AUTHOR(s): Richard D. Rechtien, David M. Stewart, Thom Cavanaugh

(15) 8. CONTRACT OR GRANT NUMBER(s): DAHC 04-74-G-0004, DAAG 29-76-G-0006

9. PERFORMING ORGANIZATION NAME AND ADDRESS

10. PROGRAM ELEMENT, PROJECT, TASK AREA & WORK UNIT NUMBERS

11. CONTROLLING OFFICE NAME AND ADDRESS
U. S. Army Research Office
Post Office Box 12211
Research Triangle Park, NC 27709

(11) 12. REPORT DATE: 30 November 76

13. NUMBER OF PAGES: 87

14. MONITORING AGENCY NAME & ADDRESS (if different from Controlling Office)

(12) 89 p.

15. SECURITY CLASS. (of this report): Unclassified

15a. DECLASSIFICATION/DOWNGRADING SCHEDULE: NA

16. DISTRIBUTION STATEMENT (of this Report)

Approved for public release; distribution unlimited.

17. DISTRIBUTION STATEMENT (of the abstract entered in Block 20, if different from Report)

NA

(18) ARO (19) 10878.2-E

18. SUPPLEMENTARY NOTES

The findings in this report are not to be construed as an official Department of the Army position, unless so designated by other authorized documents.

19. KEY WORDS (Continue on reverse side if necessary and identify by block number)

cavities, voids, seismic detection, surface waves

20. ABSTRACT (Continue on reverse side if necessary and identify by block number)

Seismic signatures of void and mud-filled subterranean cavities are presented. The results imply that cavity interference with deep penetrating surface waves is the cause for the manifestation of diagnostic seismic events indicative of voids.

DD FORM 1 JAN 73 1473 EDITION OF 1 NOV 65 IS OBSOLETE

Unclassified

410048

CONTENTS

ILLUSTRATIONS

ILLUSTRATIONS (con't)

SECTION ONE

THEORETICAL STUDIES

ON CAVITY DETECTION BY SEISMOLOGY

INTRODUCTION

Over the last decade there has been only a few published studies on the feasibility of using seismology for cave detection. Though the literature is limited, the results have varied widely. Cook (1964) postulated that S-waves should strongly reflect off of large, brine cavities, since Zoeppritz equations predict a total energy return for shear waves reflected from rock-brine boundaries. He succeeded in developing a technique for generating good S-waves, but the quality of the reflections from the cavities was poor. However, he did find amplitude attenuation for the portion of the P-wave which had passed through the cavity in comparison to the portion that had missed it. This anomaly was called the seismic amplitude "shadow".

Watkins, Godson, and Watson (1967) investigated three phenomena possibly associated with near-surface cavities; free oscillations of cave walls, seismic amplitude "shadow" zones, and anomalous delays in arrival times. A reflection traverse over a lava tunnel in the Pisgah lava flow produced long-lived oscillations. Because they vibrated at a set frequency, they were referred to as cavity resonance. Watkins *et. al*. contended that this resonance was in agreement with the radial oscillations predicted by Biot (1952) for a cylindrical bore in an elastic solid. Above the Kana-a lava flow, they discovered some clear amplitude anomalies in the "shadow" zone, but cavity resonance was not well-defined. At the Nevada test site, the underground nuclear nuclear explosion U4B had produced a rubble-filled chimney whose roof was only 30 meters below the surface. The volume of shattered and fractured rock extended to a depth of almost half a kilometer. Again they recorded some amplitude anomalies and some possible resonance. In addition, they found delays

in arrival times for the portion of the wave that had propagated through the chimney. Godson and Watkins (1968) attempted to use cavity resonance to map a cave system causing severe leaks beneath Anchor Reservoir in Wyoming. They recorded some continuous vibrations thought to be resonance, but they did not report any success in correlating these with cavities.

The field work done by Rechtien for this project consisted of seismic lines laid across several caves in east central Missouri. No periodic, long-lived signals that could be described as resonance were recorded. However, some possible reflections from the roof of a large chamber within the Cathedral Caverns complex were detected. There was also some horizontal particle motion that appeared to be polarized parallel to the sides of this chamber and its single access tunnel (Rechtien and Stewart, 1975). Additional studies in this area discovered some apparent time delays within the seismic "shadow" zone for signals reflected from a deeper horizon.

The problems that the theoretical portion of this research project attempted to solve were: (1) why should cavity resonance be so distinct at one location and weak or nonexistent at another; (2) what are the reasons for the anomalous amplitude and time delays for signals recorded above some caves; and (3) how can the seismic signature of a cavity be enhanced and more easily recognized on a seismogram? Several theoretical approaches were employed in an attempt to answer these questions. In solving the wave equation analytically in various coordinate systems, Stewart (1972) was able to examine the theoretical aspects of radial oscillations of the cavity and the interaction of this resonance with the earth's surface. Cavanaugh, Stewart, and Rechtien (1975)

considered several types of cavity surface waves as being the possible source of resonance found above some caves. Flexural waves, which would be formed if the cavity's roof behaved as a vibrating, thin plate, were also investigated as a possible source. Finally, wave scatter was thought to be the cause of the anomalies found in the "shadow" zone. To substantiate this hypothesis, both analytical and numerical solutions to the scatter problem were studied.

VIBRATIONAL MODES OF SPHERICAL CAVITIES

The first systematic attempt to theoretically investigate the possibility of cavity resonance was by Stewart (1971). If, in fact, the phenomenon reported by Watkins *et. al.* was true resonance, an understanding of it would be obtained by mathematical analysis of simple idealized void cavity shapes via the separation of variable method for solving the wave equation.

Stewart identified 113 possible cavity shapes describable through coordinate surfaces of the 11 coordinate systems in which the scalar wave equation can be separated. He ranked these surfaces in order of mathematical complexity. The simplest bounded cavity shapes were found to be the sphere, the prolate spheroid, and the oblate spheroid. He concentrated his analysis upon these three.

The pertinent conclusions of his work were:

1. Mathematically, resonance cannot exist for void cavities *per se*.

2. If resonance of any kind is to be observed over a void, it has to be the interaction between the cavity and the land surface above, not a function of the cavity alone.

3. The resonance postulated between a cavity and the land surface was not demonstrated by Stewart to have any physical meaning for spherical and spheroidal cavities.

The conclusion drawn from this work was that the development of a practical technique for the identification of cavities by seismic means was not likely to depend on the measurable presence of resonance, but will more likely be based upon other wave phenomena.

CAVITY SURFACE WAVES

Rayleigh Waves

Watkins *et. al.* proposed that the radial oscillations of a cylinder predicted by the work of Biot was an adequate explanation for the resonance that they had detected above a lava tube. Since Biot's discussion of waves on cylindrical voids and the derivation completed for this study closely parallel the Rayleigh wave problem, it will be useful to look at the assumptions and procedures used to solve this problem.

The question that Lord Rayleigh formulated and answered was this: If there existed a plane wave that travelled along the plane interface between an elastic, isotropic, homogeneous solid and a void, what would be its equations of motion? In order to make this problem solvable, it also had to be assumed that the wave attenuated away from the boundary. Such a wave was later found to actually propagate within the earth—the Rayleigh wave. The following discussion of the Rayleigh wave derivation is after Kolsky (1963).

The boundary between the solid and the void will be the xy-plane with the z-axis positive towards the interior of the solid (see Figure 1). The plane wave will move in the positive x-direction with all particle motion restricted to the xz-plane. By Helmholtz Theorem (Morse and Feshback, 1953) the displacement vector $\overline{U}$ can be written

$$\overline{U} = \nabla\Phi + \nabla \times \overline{\Psi} \qquad \text{where} \quad \nabla\cdot\overline{\Psi} = 0,$$

which becomes in two-dimensions

$$\overline{U} = (\Phi_{,x} - \Psi_{,z})\hat{i} + (\Phi_{,z} + \Psi_{,x})\hat{k}.$$

$\overline{U}$ can also be written

$$\overline{U} = U^{(x)}\hat{i} + U^{(z)}\hat{k},$$

and this implies

$$U^{(x)} = \Phi_{,x} - \Psi_{,z} \tag{1}$$

$$U^{(z)} = \Phi_{,z} + \Psi_{,x}. \tag{2}$$

The wave equations in terms of displacement are

$$\rho U^{(x)}_{,tt} = (\lambda + \mu)\Theta_{,x} + \mu\nabla^2 U^{(x)} \tag{3}$$

$$\rho U^{(z)}_{,tt} = (\lambda + \mu)\Theta_{,z} + \mu\nabla^2 U^{(z)}. \tag{4}$$

By substituting the set of equations (1) and (2) into (3) and (4) respectively, and by grouping terms, we get

$$\left(\Phi_{,tt} - \{(\lambda + 2\mu)/\rho\}\nabla^2\Phi\right)_{,x} - \left(\Psi_{,tt} - (\mu/\rho)\nabla^2\Psi\right)_{,z} = 0$$

$$\left(\Phi_{,tt} - \{(\lambda + 2\mu)/\rho\}\nabla^2\Phi\right)_{,z} - \left(\Psi_{,tt} - (\mu/\rho)\nabla^2\Psi\right)_{,x} = 0.$$

These two equations will be satisfied if and only if

$$\Phi_{,tt} - \{(\lambda + 2\mu)/\rho\}\nabla^2\Phi = 0$$

$$\Psi_{,tt} - (\mu/\rho)\nabla^2\Psi = 0,$$

or

$$\Phi_{,tt} = C_1^2\nabla^2\Phi \quad \text{where} \quad C_1 = \{(\lambda + 2\mu)/\rho\}^{\frac{1}{2}} \tag{5}$$

$$\Psi_{,tt} = C_2^2\nabla^2\Psi \quad \text{where} \quad C_2 = (\mu/\rho)^{\frac{1}{2}}. \tag{6}$$

C_1 and C_2 are the velocities of the P- and S-wave, respectively. The general solutions to the above equations are

$$\Phi = F(z)\exp\{i(\omega t - kx)\} \tag{7}$$

$$\Psi = G(z)\exp\{i(\omega t - kx)\}, \tag{8}$$

when it is assumed that $\underline{\Phi}$ and $\underline{\Psi}$ are harmonic functions. It also follows from equations (5) and (7) that

$$F(z) = Ae\exp\{-z(k^2 - \omega^2/C_1^2)^{\frac{1}{2}}\} + A^*\exp\{z(k^2 - \omega^2/C_1^2)\}^{\frac{1}{2}}.$$

The term $A^*\exp\{z(k^2 - \omega^2/C_1^2)\}^{\frac{1}{2}}$ implies that F(z), and therefore $\underline{\phi}$, increases exponentially with depth. This is contrary to the original assumption that the wave vanishes with depth. Hence, to meet this initial condition, A^* must be zero. The formula for G(z) is abbreviated in a similar fashion and the complete solutions for (5) and (6) are

$$\phi = A\exp\{-Qz + i(\omega t - kx)\} \qquad \text{where} \quad Q = (k^2 - k_1^2)^{\frac{1}{2}} \tag{9}$$

$$\Psi = B\exp\{-Sz + i(\omega t - kx)\} \qquad \text{where} \quad S = (k^2 - k_2^2)^{\frac{1}{2}}. \tag{10}$$

The boundary between the solid and the void must be stress-free and this iplies that $\sigma_{(zz)}$ and $\sigma_{(zx)}$ are equal to zero. From the general relationship,

$$\sigma_{(ik)} = \lambda\theta\delta_{ik} + 2\mu e_{(ik)},$$

it can be shown that in rectangular coordinates that

$$\sigma_{(zz)} = (\lambda + 2\mu)\phi_{,zz} + \lambda\phi_{,xx} + 2\mu\Psi_{,xz} \tag{11}$$

$$\sigma_{(zx)} = \mu(2\phi_{,xz} - \Psi_{,zz} + \Psi_{,xx}). \tag{12}$$

Setting the left side of these statements equal to zero and substituting in the designated partial derivatives of (9) and (10), it develops that

$$A\{(\lambda + 2\mu)Q^2 + \lambda k^2\} + B\{2\mu ki s\} = 0 \tag{13}$$

$$A\{2Qki\} - B\{k^2 + S^2\} = 0. \tag{14}$$

Substituting the second equation into the first gives

$$4\mu QSk = \{(\lambda + 2\mu)Q^2 - \lambda k^2\}(k^2 + S^2). \tag{15}$$

By recalling that

$$Q = (k^2 - k_1^2)^{\frac{1}{2}}$$

$$S = (k^2 - k_2^2)^{\frac{1}{2}}$$

and expanding, equation (15) is transformed to

$$\zeta^6 - 8\zeta^4 + (24 - 16\alpha^2)\zeta^2 + (16\alpha^2 - 16) = 0$$

with

$$\zeta^2 = (k_2/k) = (C/C_2)$$

$$\alpha^2 = (1 - 2\sigma)/(2 - 2\sigma).$$

This is a cubic equation in terms of ζ^2, which can be solved when σ, Poisson's ratio, is known for the solid. $\underline{C}$ is the velocity of the Rayleigh wave and it is obtained from the formula for ζ. This velocity is independent of frequency, which indicates that there is no dispersion. Hence, when values are given for $\underline{\sigma}$, $\underline{\lambda}$, and $\underline{\mu}$, it is possible to calculate $\underline{C}_1$, $\underline{C}_2$, $\underline{C}$, $\underline{\zeta}$, $\underline{Q}$, and $\underline{S}$. With these quantities available, particle motion can be studied. By inserting the designated partial derivatives of (9) and (10) into equations (1) and (2), and noting that from (14) that

$$B = (2AQki)/(k^2 + S^2),$$

the following equations for the components of the displacement vector are obtained;

$$U^{(x)} = Ak\{\exp(-Qz) - 2QS\exp(-Sz)/(k^2 + S^2)\}\{\sin(\omega t - kx)\} \qquad (16)$$
$$- Aki\{\exp(-Qz) - 2QS\exp(-Sz)/(k^2 + S^2)\}\{\cos(\omega t - kx)\}$$

$$U^{(z)} = -AQ\{\exp(-Qz) - 2k^2\exp(-Sz)/(k^2 + S^2)\}\{\cos(\omega t - kx)\} \qquad (17)$$
$$+ AQi\{\exp(-Qz) - 2k^2\exp(-Sz)/(k^2 + S^2)\}\{\sin(\omega t - kx)\}.$$

Both components are complex numbers and the usual argument made at this point is that since only real solutions are desired, all values associated with the imaginary term $\underline{i}$ can be neglected. This is an invalid statement. As an example, in

$$a + bi$$

both a and b are real numbers, even though this is a complex expression. The imaginary term i acts as a label that partitions the two real numbers a and b, maintains proper separation during mathematical operations, and controls their signs. In equations (16) and (17), both the real solutions

$$U^{(x)} = Ak\{\exp(-Qz) - 2QS\exp(-Sz)/(k^2 + S^2)\}\{\sin(\omega t - kx)\}$$

$$U^{(z)} = -AQ\{\exp(-Qz) - 2k^2\exp(-Sz)/(k^2 + S^2)\}\{\cos(\omega t - kx)\}$$

and the imaginary solutions

$$U^{(x)} = -Ak\{\exp(-Qz) - 2QS\exp(-Sz)/(k^2 + S^2)\}\{\cos(\omega t - kx)\}$$

$$U^{(z)} = AQ\{\exp(-Qz) - 2k^2\exp(-Sz)/(k^2 + S^2)\}\{\sin(\omega t - kx)\}$$

are correct. Each set of equations predicts the behavior of a surface wave that has retrograde particle motion with respect to the direction of propagation. The only difference is that they are 90 degrees out of phase in relation to each other. This inability to discount the imaginary portion of the equations at any step of the derivation, except perhaps for the last one, will be an important factor in later derivations.

Axial Surface Waves on a Cylinder

Biot considered the possibility of a wave propagating along the length of a bore located within an elastic, infinite medium. This disturbance was to be symmetric with respect to the axis of the cylindrical void and largely restricted to its surface. As with the Rayleigh wave problem, the particle motion was restricted to a plane. In this case, it was the rz-plane defined in the cylindrical coordinate system (see Figure 1). From the Helmholtz equation and the formulation of the divergence and the curl in this system, the following displacement vector

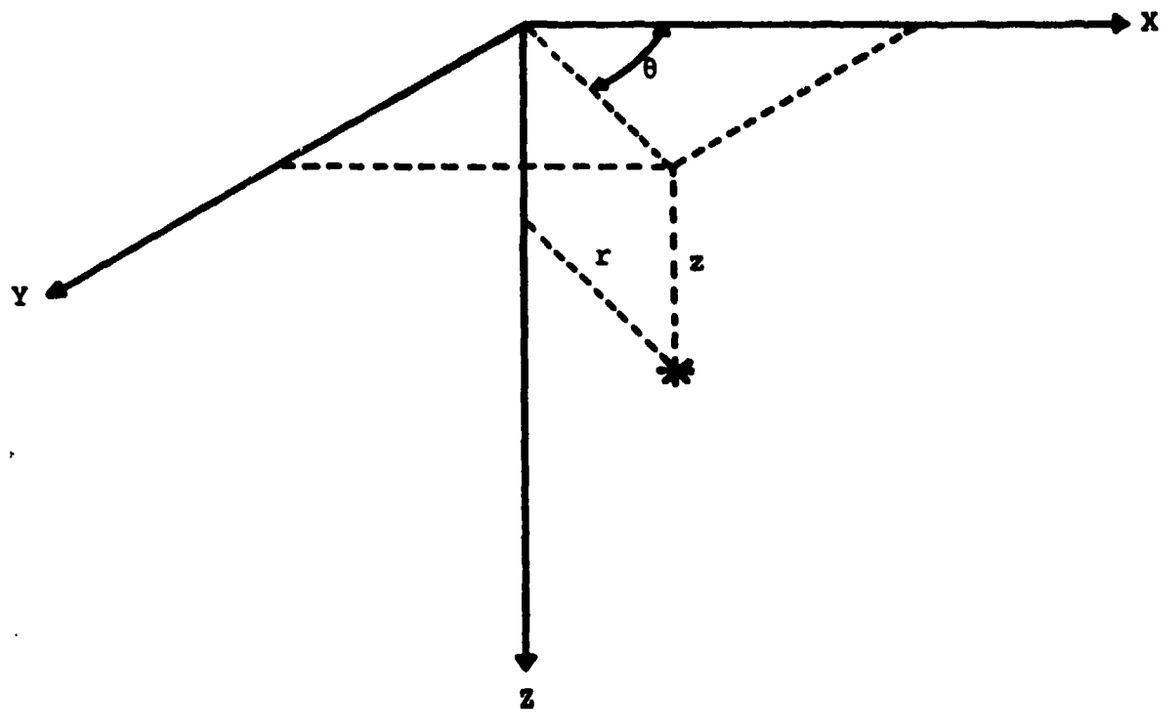

Figure 1. Cylindrical coordinates superimposed on the right-handed rectangular coordinate system.

is obtained;

$$\bar{U} = (\phi_{,r} - \psi_{,z})e_r + (\phi_{,z} + \psi/r + \psi_{,r})e_z.$$

Therefore,

$$U^{(r)} = \phi_{,r} - \psi_{,z} \tag{1}$$

$$U^{(z)} = \phi_{,z} + \psi/r + \psi_{,r}.$$

In rectangular coordinates, the wave equations are expressed as

$$\nabla^2\phi = (1/C_1^2)\phi_{,tt} \tag{2}$$

$$\nabla^2\bar{\psi} = (1/C_2^2)\bar{\psi}_{,tt}. \tag{3}$$

In cylindrical form, (2) becomes

$$\phi_{,rr} + \phi_{,r}/r + \phi_{,zz} = \phi_{,tt}/C_1^2. \tag{4}$$

Due to the axial symmetry, the vector $\bar{\psi}$ is restricted to the xy-plane and its components may be written

$$\psi^{(x)} = -\psi\sin\theta \tag{5}$$

$$\psi^{(y)} = \psi\cos\theta. \tag{6}$$

The x- and y-components of equation (3) are

$$\psi^{(x)}_{,rr} + \psi^{(x)}_{,r} + \psi^{(x)}_{,\theta\theta}/r^2 + \psi^{(x)}_{,zz} = \psi^{(x)}_{,tt}/C_2^2 \tag{7}$$

$$\psi^{(y)}_{,rr} + \psi^{(y)}_{,r} + \psi^{(y)}_{,\theta\theta}/r^2 + \psi^{(y)}_{,zz} = \psi^{(y)}_{,tt}/C_2^2. \tag{8}$$

Substituting (5) into equation (7) gives

$$\psi_{,rr} + \psi_{,r}/r - \psi/r^2 + \psi_{,zz} = \psi_{,tt}/C_2. \tag{9}$$

The same result is obtained when (6) is substituted into (8). Solutions now must be found for equations (4) and (9) by separation of variables. Let

$$\Phi(r,z,t) = R(r)Z(z)\exp(-i\omega t).$$

The replacing of Φ in equation (4) with this function results in the following ordinary differential equations;

$$Z'' - k^2 Z = 0$$

$$R'' + R'/r - (k^2 - \omega^2/C_1^2)R = 0.$$

The solution to the first equation is that of a wave travelling in the positive z-direction;

$$Z = A^* \exp(i\omega z).$$

The second differential equation has solutions in terms of the Modified Bessel Functions, I_0 and K_0 (McLachlan, 1955). Only K_0 approaches zero as the radius goes to infinity. Since it is assumed that the wave attenuates away from the boundary, I_0 is not considered in the answer. Therefore,

$$R = A^{**} K_0\left((k^2 - \omega^2/C_1^2)^{\frac{1}{2}} r\right)$$

and the total solution to (4) is written

$$= AK_0(mr)\exp\{i(kz - \omega t)\}$$

where

$$m = k(1 - \zeta_1^2)^{\frac{1}{2}}$$

$$\zeta_1 = v/C_1.$$

The value v is the phase velocity. The solution to (9) is found in a similar fashion with one of the resulting differential equations being in the form that has solutions containing the Modified Bessel Functions, I_1 and K_1. At this point, Biot changed from the exponentials to sines and cosines, making the solutions to equations (4) and (9)

$$\phi = AK_0(mr)\cos(kz - \omega t) \tag{10}$$

$$\psi = BK_1(nr)\sin(kz - \omega t) \tag{11}$$

where

$$m = k(1 - \zeta_1^2)^{\frac{1}{2}} \qquad \text{with} \quad \zeta_1 = v/C_1$$

$$n = k(1 - \zeta_2^2)^{\frac{1}{2}} \qquad \text{with} \quad \zeta_2 = v/C_2.$$

Using these two solutions, properties of Modified Bessel Functions, and the assumptions that $\sigma_{(rr)}$ and $\sigma_{(rz)}$ vanish on the interface, it can be shown that

$$4(1 - \zeta_2^2)^{\frac{1}{2}}\{1/(\pi D/\lambda)(1 - \zeta_2^2)^{\frac{1}{2}} + K_0\left((\pi D/\lambda)(1 - \zeta_2^2)^{\frac{1}{2}}\right)/K_1\left((\pi D/\lambda)(1 - \zeta_2^2)^{\frac{1}{2}}\right)\} \tag{12}$$

$$- 2(2 - \zeta_2^2)(1 - \zeta_2^2\alpha^2)^{\frac{1}{2}}/(\pi D/\lambda)(1 - \zeta_2^2\alpha^2)$$

$$- \{(2 - \zeta_2^2)/(1 - \zeta_2^2\alpha^2)^{\frac{1}{2}}\}\{K_0\left((\pi D/\lambda)(1 - \zeta_2^2\alpha^2)^{\frac{1}{2}}\right)/K_1\left((\pi D/\lambda)(1 - \zeta_2^2\alpha^2)^{\frac{1}{2}}\right)\} = 0,$$

where

$$\alpha^2 = (1 - 2\sigma)/(2 - 2\sigma)$$

$$\zeta_2 = v/C_2$$

D = diameter of cavity

λ = wavelength.

It also can be shown that when the partial derivatives of equations (10) and (11) are substituted into equations (1), the result is

$$U^{(r)} = A\{-mK_1(ma) - 2k(1 - \zeta_1^2)^{\frac{1}{2}}K_1(ma)/(2 - \zeta_2^2)\}\cos(kz - \omega t) \tag{13}$$

$$U^{(z)} = A\{-kK_0(ma) + 2(1/n + 1)(1 - \zeta_1^2)^{\frac{1}{2}}K_1(ma)/a(2 - \zeta_2^2) \tag{14}$$

$$+ 2(1 - \zeta_1^2)^{\frac{1}{2}}K_1(ma)K_0(na)/(2 - \zeta_2^2)K_1(na)\}\sin(kz - \omega t),$$

where a is the radius of the cavity.

The formulas given in (12), (13), and (14) are important for several reasons. They show the similarity between Biot's work and the derivation for the Rayleigh wave. They also indicate whether cylindrical

surface waves are applicable to the problem of cavity resonance. In (12), when Poisson's ratio $\underline{\sigma}$ is given, the equation becomes a function of λ/D and ζ_2. This formula shows that unlike the Rayleigh wave, the cylindrical surface wave suffers dispersion, with the wave velocity dependent on the frequency. As with the Rayleigh wave, the particle motion is elliptical. However, equations (13) and (14) demonstrate that this motion can advance in relation to direction of propagation as well as be retrograde. This is a function of the circumference of the cavity.

Watkins *et. al.* used the equation

$$f = C_2/1.55D$$

to calculate the theoretical frequency of radial resonance for a cavity when dispersion was at a minimum. This was obtained from the plot of ζ_2 versus λ/D, whose values were defined by (12). However, the components of the displacement vector and the original statement of the problem both indicate that this is not a standing wave phenomenon, but a wave that moves parallel to the z-axis. As with the Rayleigh case, to have waves possessing set frequencies sweep past a single point over an extended period of time, it is necessary for these waves to be continuously generated. This is not the case for energy dispersed by a dynamite explosion. Consequently, Biot's derivation cannot explain the definite, long-lived oscillations recorded by Watkins *et. al.* above some cavities. A different interpretation must be made.

Circumferential Surface Waves on a Cylinder

Since resonance was found over relatively shallow caves and because surface waves attenuate away from the wall of a cavity, it was thought that a different type of surface wave might be the solution to the problem.

It was believed that resonance may be induced by cylindrical surface waves travelling about the circumference of the cavity. With this form of wave, the frequency and strength of oscillations recorded at the earth's surface would be a function of; the wave's velocity, the cavity's circumference, the depth to the cave, and the types of interference produced by the different surface waves. If this theory were correct, it would mean that a great deal could be told about the cavity by the traces of the seismogram. It would also explain why resonance had not been recorded over deep cavities.

The statement of the problem is similar to the previous two examples. It is assumed that there is a cylindrical bore in an elastic, infinite solid, which has a symmetric wave moving about its circumference. The particle motion is restricted to the rθ-plane and it attenuates away from the surface of the cavity.

By writing the divergence and the curl of the Helmholtz Theorem in terms of cylindrical coordinates and invoking the condition that no motion can occur outside of the rθ-plane, the components of the displacement vector $\bar{U}$ are expressed as

$$U^{(r)} = \phi_{,r} + \psi_{,\theta}/r \qquad (1)$$

$$U^{(\theta)} = \phi_{,\theta}/r + \psi_{,r}.$$

After Eringer (1967), the most general expression of the wave equation is

$$\rho\bar{U}_{,tt} = (\lambda + 2\mu)\nabla\Theta - \mu(\nabla \times \nabla \times \bar{U}). \qquad (2)$$

The dilatation $\underline{\Theta}$ is given by

$$\Theta = \nabla\cdot\bar{U}$$

$$\Theta = U^{(r)}/r + U^{(r)}_{,r} + U^{(\theta)}_{,\theta}/r$$

$$0 = (\phi_{,r} + \psi_{,\theta}/r)/r + (\phi_{,rr} - \psi_{,\theta}/r^2 + \psi_{,\theta r}/r) + (\phi_{,\theta\theta}/r - \psi_{,\theta r})/r$$

$$\theta = \phi_{,r}/r + \phi_{,rr} + \phi_{,\theta\theta}/r^2$$

$$0 = \nabla^2\phi. \tag{3}$$

This demonstrates that the dilatation is equal to the Laplacian of the scalar potential ϕ. The curl of U is given by

$$\nabla \times \nabla \times \bar{U} = (U^{(\theta)}_{,\theta}/r^2 + U^{(\theta)}_{,r\theta}/r - U^{(r)}_{,\theta\theta}/r^2)e_r + (U^{(\theta)}/r^2 - U^{(\theta)}_{,r}/r - U^{(\theta)}_{,rr} - U^{(r)}_{,\theta}/r^2 + U^{(r)}_{,r\theta}/r)e_\theta. \tag{4}$$

By substituting equation (3), equation (4), and the partial derivatives of the components of the displacement vector into (2), the following equations are obtained;

$$\rho U^{(r)}_{,tt} = (\lambda + 2\mu)(\nabla^2\phi)_{,r} + (\mu/r)(\psi_{,rr} + \psi_{,r}/r + \psi_{,\theta\theta}/r^2)_{,\theta}$$

$$\rho U^{(\theta)}_{,tt} = \{(\lambda + 2\mu)/r\}(\nabla^2\phi)_{,\theta} - \mu(\psi_{,rr} + \psi_{,r}/r + \psi_{,\theta\theta}/r^2)_{,r}.$$

By inserting the values of $U^{(r)}$ and $U^{(\theta)}$ given in (1) and observing that the Laplacian of $\underline{\Psi}$ is present on the right side of the above equations, we get

$$\rho(\phi_{,tt})_{,r} + (\rho/r)(\psi_{,tt})_{,\theta} = (\lambda + 2\mu)(\nabla^2\phi)_{,r} + (\mu/r)(\nabla^2\psi)_{,\theta}$$

$$(\rho/r)(\phi_{,tt})_{,\theta} - \rho(\psi_{,tt})_{,r} = \{(\lambda + 2\mu)/r\}(\nabla^2\phi)_{,\theta} - \mu(\nabla^2\psi)_{,r}$$

or

$$\left(\phi_{,tt} - \{(\lambda + 2\mu)/\rho\}\nabla^2\phi\right)_{,r} + (1/r)\left(\psi_{,tt} - (\mu/\rho)\nabla^2\psi\right)_{,\theta} = 0$$

$$(1/r)\left(\phi_{,tt} - \{(\lambda + 2\mu)/\rho\}\nabla^2\phi\right)_{,\theta} - \left(\psi_{,tt} - (\mu/\rho)\nabla^2\psi\right)_{,r} = 0.$$

These will be valid if and only if the following equations hold;

$$\phi_{,tt} = C_1^2\nabla^2\phi \qquad \text{where} \quad C_1 = \{(\lambda + 2\mu)/\rho\}^{1/2} \tag{5}$$

$$\Psi_{,tt} = C_2^2 \nabla^2 \Psi \qquad \text{where} \quad C_2 = (\mu/\rho)^{\frac{1}{2}} \tag{6}$$

These are the two scalar wave equations. We have shown that they are the same in cylindrical coordinates as those derived in the Rayleigh wave problem. The next step is to solve equation (5) by separation of variables. The answer to equation (6) will be of the same form. Let Φ have a solution that is harmonic with time. Hence,

$$\Phi = R(r)\Theta(\theta)\exp(i\omega t).$$

Substituting into (5) results in the expression

$$\nabla^2(R\Theta) + k_1^2 R\Theta = 0 \qquad \text{where} \quad k_1 = \omega/C_1.$$

Expanding the Laplacian in cylindrical coordinates gives the equation

$$r^2 R_{,rr}/R + rR_{,r}/R + r^2 k_1^2 = -\Theta_{,\theta\theta}/\Theta = m^2$$

where m is the integration constant. This can be separated into two ordinary differential equations;

$$\Theta_{,\theta\theta} + m^2\Theta = 0$$

$$r^2 R_{,rr} + rR_{,r} + (r^2 k_1^2 - m^2)R = 0.$$

The first equation has the general solution

$$\Theta = A^* \exp(-im\theta) + B^* \exp(im\theta).$$

The negative exponent term is for a wave moving about the cavity counterclockwise and the positive exponent is for one moving clockwise. Choosing the counterclockwise wave gives the solution

$$\Theta = A^* \exp(-im\theta).$$

The second equation is in the form of

$$Z^2 W_{,ZZ} + ZW_{,Z} + (Z^2 - \gamma^2)W = 0,$$

which is the differential equation for the Hankel Function. Therefore,

the general solution for the second differential equation is

$$R = A^{**}H_m^{(2)}(rk_1) + B^{**}H_m^{(1)}(rk_1).$$

According to Butkov (1968), when $\exp(i\omega t)$ is chosen as the time harmonic portion of the original function, it is necessary to choose the Hankel Function of the second kind so as to satisfy the Sommerfeld Radiation condition. Since this is the only Hankel Function used throughout the derivation, the superscript will be left off. The solution for $\underline{R}$ is now written

$$R = A^{**}H_m(rk_1)$$

with the Hankel Function of the second kind defined as

$$H_m(rk_1) = J_m(rk_1) - iY_m(rk_1).$$

Therefore, the solutions for $\underline{\Phi}$ and $\underline{\Psi}$ are

$$\Phi = AH_m(rk_1)\exp\{i(\omega t - m\theta)\} \tag{7}$$

$$\Psi = BH_m(rk_2)\exp\{i(\omega t - m\theta)\}. \tag{8}$$

where

$$k_1 = \omega/C_1$$

$$k_2 = \omega/C_2.$$

Expressing the stress components $\sigma_{(rr)}$ and $\sigma_{(r\theta)}$, in terms of $\underline{\Phi}$ and $\underline{\Psi}$ results in the following two expressions;

$$\sigma_{(rr)} = (\lambda + 2\mu)(\Phi_{,rr} - \Psi_{,\theta}/r^2 + \Psi_{,\theta r}/r) + \lambda(\Phi_{,\theta\theta}/r^2 - \Psi_{,r\theta}/r + \Phi_{,r}/r + \Psi_{,\theta}/r^2) \tag{9}$$

$$\sigma_{(r\theta)} = (\mu/r^2)(2r\Phi_{,r\theta} + \Psi_{,\theta\theta} + r\Psi_{,r} - r^2\Psi_{,rr} - 2\Phi_{,\theta}). \tag{10}$$

The first derivative of the Hankel Function is

$$H_m(rk_1)_{,r} = (k_1/2)\{H_{m-1}(rk_1) - H_{m+1}(rk_1)\}.$$

The second derivative is

$$H_m(rk_1)_{,rr} = (k_1/4)\{H_{m-2}(rk_1) - 2H_m(rk_1) + H_{m+2}(rk_1)\}.$$

Using these derivatives, it is now possible to take the partials of (7) and (8) and substitute them into equations (9) and (10). For simplicity, we will adopt the following convention;

$$h_m = H_m(rk_1)$$

$$H_m = H_m(rk_2).$$

The stress components now become

$$\sigma_{(rr)} = \big(A\{(\mu k_1^2/2 + \lambda k_1^2/4)(H_{m-2} - 2H_m + H_{m+2}) - (\lambda m^2/r^2)H_m \qquad (11)$$
$$+ (\lambda k_1/2r)(H_{m-1} - H_{m+1})\} + B\{(2\mu mi/r^2)h_m$$
$$- (\mu mik_2/r)(h_{m-1} - h_{m+1})\}\big)\exp\{i(\omega t - m\theta)\}$$

$$\sigma_{(r\theta)} = \big(B\{(-\mu k_2^2/4)(h_{m-2} - 2h_m + h_{m+2}) - (\mu m^2/r^2)h_m \qquad (12)$$
$$+ (\mu k_2/2r)(h_{m-1} - h_{m+1})\} + A\{(2\mu mi/r^2)H_m$$
$$- (\mu mik_1/r)(H_{m-1} - H_{m+1})\}\big)\exp\{i(\omega t - m\theta)\}.$$

If $\underline{a}$ is the radius of the cavity, the stresses expressed above vanish when $r = a$. Given radius $\underline{a}$ and letting

$$\alpha = (\mu k_1^2/2 + \lambda k_1^2/4)(H_{m-2} - 2H_m + H_{m+2}) - (\lambda m^2/a^2)H_m$$
$$+ (\lambda k_1/2a)(H_{m-1} - H_{m+1})$$

$$\beta = (k_2^2/4)(h_{m-2} - 2h_m + h_{m+2}) + (m^2/a^2)h_m - (k_2/2a)(h_{m-1} - h_{m+1})$$

$$\gamma = (2m/a^2)H_m - (mk_1/a)(H_{m-1} - H_{m+1})$$

$$\delta = (2\mu m/a^2)h_m - (\mu mk_2/a)(h_{m-1} - h_{m+1}),$$

equations (11) and (12) become

$$0 = A\alpha + B\delta i$$

$$0 = B\beta + A\gamma i.$$

Substituting the second equation into the first results in

$$\alpha\beta = \gamma\delta. \tag{13}$$

Let

$$P = (\mu k_1^2/2 + \lambda k_1^2/4)(J_{m-2} - 2J_m + J_{m+2}) - (\lambda m^2/a^2)J_m + (\lambda k_1/2a)(J_{m-1} - J_{m+1})$$

$$Q = (\mu k_1^2/2 + \lambda k_1^2/4)(Y_{m-2} - 2Y_m + Y_{m+2}) - (\lambda m^2/a^2)Y_m + (\lambda k_1/2a)(Y_{m-1} - Y_{m+1})$$

$$R = (k_2^2/4)(j_{m-2} - 2j_m + j_{m+2}) + (m^2/a^2)j_m - (k_2/2a)(j_{m-1} - j_{m+1})$$

$$S = (k_2^2/4)(y_{m-2} - 2y_m + y_{m+2}) + (m^2/a^2)y_m - (k_2/2a)(y_{m-1} - Y_{m+1})$$

$$T = (2m/a^2)J_m - (mk_1/a)(J_{m-1} - J_{m+1})$$

$$U = (2m/a^2)Y_m - (mk_1/a)(Y_{m-1} - Y_{m+1})$$

$$V = (2\mu m/a^2)j_m - (\mu mk_2/a)(j_{m-1} - j_{m+1})$$

$$W = (2\mu m/a^2)y_m - (\mu mk_2/a)(y_{m-1} - y_{M+1}).$$

Expanding $\underline{\alpha}$, $\underline{\beta}$, $\underline{\gamma}$, and $\underline{\delta}$ into their real and imaginary parts creates the following complex formulae;

$$\alpha = P - Qi$$

$$\beta = R - Si$$

$$\gamma = T - Ui$$

$$\delta = V - Wi.$$

Substituting these into equation (13) gives

$$(PR - QS) - (QR + PS)i = (TV - UW) - (UV + TW)i.$$

These two complex expressions will be equal to one another if and only if

$$PR - QS = TV - UW \tag{14}$$

and

$$QR + PS = UV + TW. \tag{15}$$

Therefore, the ω that causes both of these equations to hold simultaneously, will be the angular frequency of the wave propagating about the circumference of the cavity. Using this frequency, it is possible to describe the particle motion. Inserting the partial derivatives of equations (7) and (8) into equations (1) gives

$$U^{(r)} = \{(Ak_1/2)(H_{m-1} - H_{m+1}) - (Bmi/r)h_m\}\exp\{i(\omega t - m\theta)\} \tag{16}$$

$$U^{(\theta)} = \{(-Ami/r)H_m - (Bk_2/2)(h_{m-1} - h_{m+1})\}\exp\{i(\omega t - m\theta)\}. \tag{17}$$

We already have that

$$0 = B\beta + A\gamma i$$

or

$$B = A(\gamma/\beta)i,$$

which indicates that

$$B = A\left[\{(UR - ST)/(R^2 + S^2)\} + \{(TR + US)/(R^2 + S^2)\}i\right].$$

Replace B in equations (16) and (17) with the above value and expand the Hankel Function into its real and imaginary parts. This changes the components of the displacement vector to

$$U^{(r)} = A\left[\{\Gamma\cos(\omega t - m\theta) - \Lambda\sin(\omega t - m\theta)\} + \{\Gamma\sin(\omega t - m\theta) + \Lambda\cos(\omega t - m\theta)\}i\right]$$

$$U^{(\theta)} = A\left[\{\Xi\cos(\omega t - m\theta) - \Omega\sin(\omega t - m\theta)\} + \{\Xi\sin(\omega t - m\theta) + \Omega\cos(\omega t - m\theta)\}i\right]$$

where

$$\Gamma = (k_1/2)(j_{m-1} - j_{m+1}) - (m/a)\{(UR - ST)/(R^2 + S^2)\}y_m$$
$$+ (m/a)\{(TR + US)/(R^2 + S^2)\}j_m$$

$$\Lambda = (-k_1/2)(Y_{m-1} - Y_{m+1}) - (m/a)\{(UR - ST)/(R^2 + S^2)\}j_m$$
$$- (m/a)\{(TR + US)/(R^2 + S^2)\}j_m$$

$$\Xi = (-m/a)Y_m - (k_2/2)\{(UR - ST)/(R^2 + S^2)\}(j_{m-1} - j_{m+1})$$
$$- (k_2/2)\{(TR + US)/(R^2 + S^2)\}(y_{m-1} - y_{m+1})$$

$$\Omega = (-m/a)J_m + (k_2/2)\{(UR - ST)/(R^2 + S^2)\}(y_{m-1} - y_{m+1})$$
$$- (k_2/2)\{(TR + US)/(R^2 + S^2)\}(j_{m-1} - j_{m+1}).$$

The values R, S, T, and U are as defined earlier and a is the radius of the cylinder. It is not possible to find the absolute values for the displacement vector $\bar{U}$, but since both components are expressed in terms of A, their amplitudes may be compared. If the constant A is negative or complex, the only change to $U^{(r)}$ and $U^{(\theta)}$ would be a phase change. There also is no loss of generality if only the real portion of the above equations is used. Therefore, the components of the displacement vector may be written

$$U^{(r)} = A\{\Gamma\cos(\omega t - m\theta) - \Lambda\sin(\omega t - m\theta)\} \qquad (18)$$

$$U^{(\theta)} = A\{\Xi\cos(\omega t - m\theta) - \Omega\sin(\omega t - m\theta)\}. \qquad (19)$$

This completes the derivation of the circumferential surface wave on a cylinder. The intention was to use these displacement formulae to define the motion of the particles along hypothetical horizons above the cavity as shown in Figure 2.

A computer program was written to numerically solve equations (14) and (15), when a, λ, and μ were given. The procedure was to set m, the mode, and vary ω iteratively until the left side of the equations

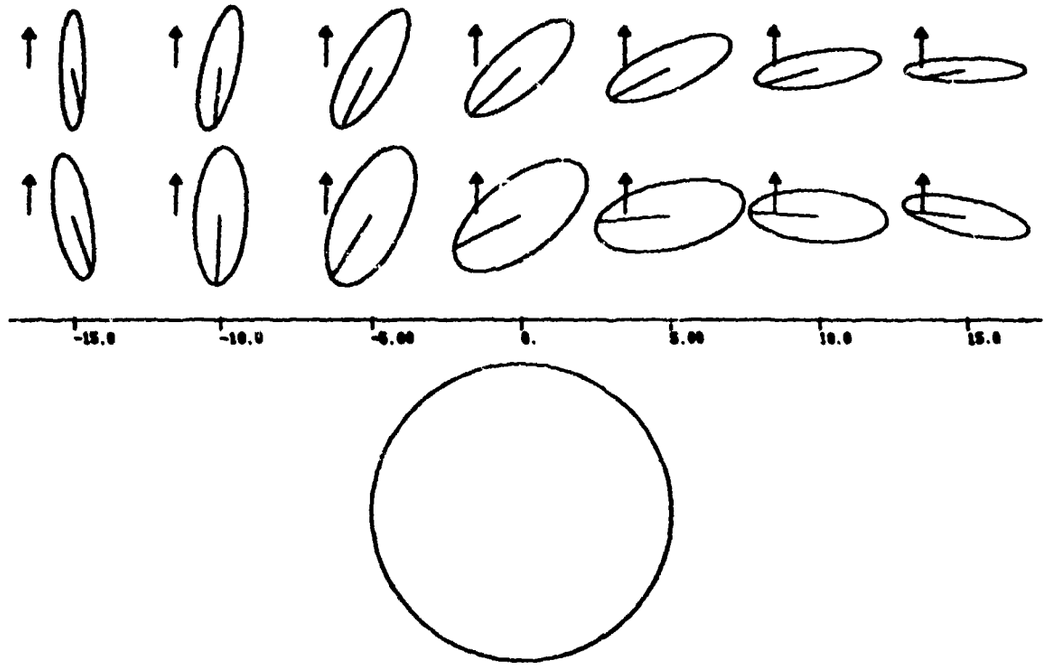

Figure 2. Possible elliptical motion and direction of rotation of points along two hypothetical lines above a cavity.

equalled the right. It was found to be impossible to satisfy both equations simultaneously. Even when imaginary equation (15) was neglected, the angular frequency generated for a cavity of reasonable size, resulted in a wave whose velocity was much greater than that of a P-wave. Since it was assumed in the derivation that the cavity surface wave would be a combination of compressional and shear motion, it would be impossible for a wave to propagate at this speed.

This conclusion is in agreement with Stilke, who completed a three-dimensional version of Biot's problem. He found that the cylindrical surface wave could spiral about a tube as illustrated in Figure 3, but that for all modes except $m = 1$, no wave could have only $r\theta$-motion. For $m = 1$, this occurred when the wavelength approached infinity or the cylinders radius approached zero. The results of our derivation and those of Stilke imply that circumferential surface waves on a cylinder cannot exist and therefore cannot be the cause of apparent cavity resonance.

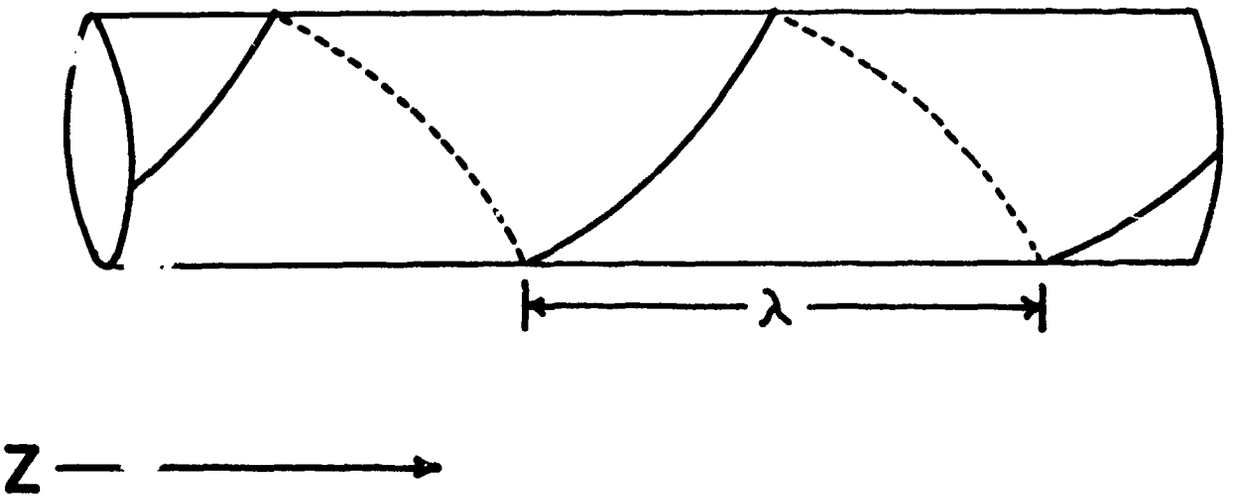

Figure 3. Lines of equal phase for a cavity surface wave (after Stilke).

FLEXURAL WAVES

With the failure of cavity surface waves to explain cavity resonance, the next hypothesis investigated was the "drumhead" effect as suggested by Finn Bronner (personal communication). The existence of such an effect would imply that the roof of a cave oscillates vertically with little or no horizontal components of motion. As a first step in studying this possible phenomenon, the behavior of a vibrating membrane was examined.

Vibrating Membrane

The equation of motion for a round membrane in cylindrical coordinates is

$$\xi_{,rr} + \xi_{,r}/r - \Gamma^2 \xi_{,tt} = 0 \qquad (1)$$

where

$$\Gamma^2 = m/T,$$

with

m = mass per unit area

T = total tension.

Using the boundary condition for $\xi(r,t)$ of

$$\xi(a,t) = 0$$

for all time t and membrane radius a, and the intitial condition

$$\xi(0,0) = \xi_0,$$

it can be shown that

$$J_0(\omega a/\Gamma) = 0.$$

The radial frequency of the membrane will be that ω which satisfies this equation (Churchill, 1963). There are a number of implicit assumptions that have to be made to solve this proble. They are;

1) vibrations occur within a vacuum,

2) there is no damping,

3) the system is perfectly elastic,

4) amplitudes are small,

5) deformation due to gravity may be neglected,

6) the membrane is thin (surface of "points"), and

7) tension is constant at all times, even during deformation.

The first five assumptions present no problems, since they are used extensively in wave propagation problems whose results have been shown to be reliable. The last two assumptions cannot be met. No cavity roof can be thought of as being a surface of points and the forces that support a roof are not analogous to tension. Therefore, equation (1) is not applicable for calculating frequencies found over caves. The next approach was to look at the equations of a vibrating, thin plate.

Vibrating Plate

The general equation of motion for a thin plate is

$$\nabla^4 \xi + (1/C^2)\xi_{,tt} = 0 \qquad (2)$$

where

$$C = (Eh^2)/12\rho(1 - \sigma^2), \qquad (3)$$

with

E = Young's Modulus

h = thickness of plate

ρ = density

σ = Poisson's Ratio.

In the solutions that follow, all the assumptions are the same as for the membrane problem, except that the last two are replaced by one assumption —the plate is thin. What this means is that within the plate there is

a neutral surface which is neither compressed nor extended as the plate bends, and that the motion of this hypothetical surface closely mirrors the movement of the plate's top and bottom surfaces. There is no exact definition of when a plate can no longer be considered thin, but perhaps it is when the plate's behavior can not be predicted theoretically. In seismology, the oscillations associated with plates are called flexural waves, and they are found to exist over frozen lakes (Ewing, Jardetzky, and Press, 1957) and in desert environments where a crust of caliche has formed (Richter, 1958). The question is whether the resonance found by Watkins *et. al.* over a lava tunnel and at an underground nuclear test site was due to the generation of flexural waves.

To solve equation (2) for a circular plate, the boundary conditions for $\xi(r,\theta)$ are made to be

$$\xi(a,\theta) = 0$$

$$\xi(a,\theta)_{,r} = 0,$$

where a is the radius of the plate. The result is

$$J_m(\lambda)I_{m+1}(\lambda) + J_{m+1}(\lambda)I_m(\lambda) = 0,$$

which has n solutions for each integer m. $\lambda_{m,n}$ is found by a series expansion and is constant for set values of m and n. The equation for the angular frequency is

$$\omega_{m,n} = (h\lambda_{m,n}/a^2)\{E/12\rho(1 - \sigma^2)\}^{\frac{1}{2}}. \qquad (4)$$

Figure 4 has some examples of modes of vibration for a circular plate (McLachlan, 1951).

Landau and Lifshitz (1959) did a similar problem for a rectangular plate with sides of length a and b. The boundary conditions are

$$\left.\begin{aligned}\xi(x,y) &= 0\\ \xi(x,y)_{,x} &= 0\end{aligned}\right\} \quad \text{for } x = 0 \text{ and } a$$

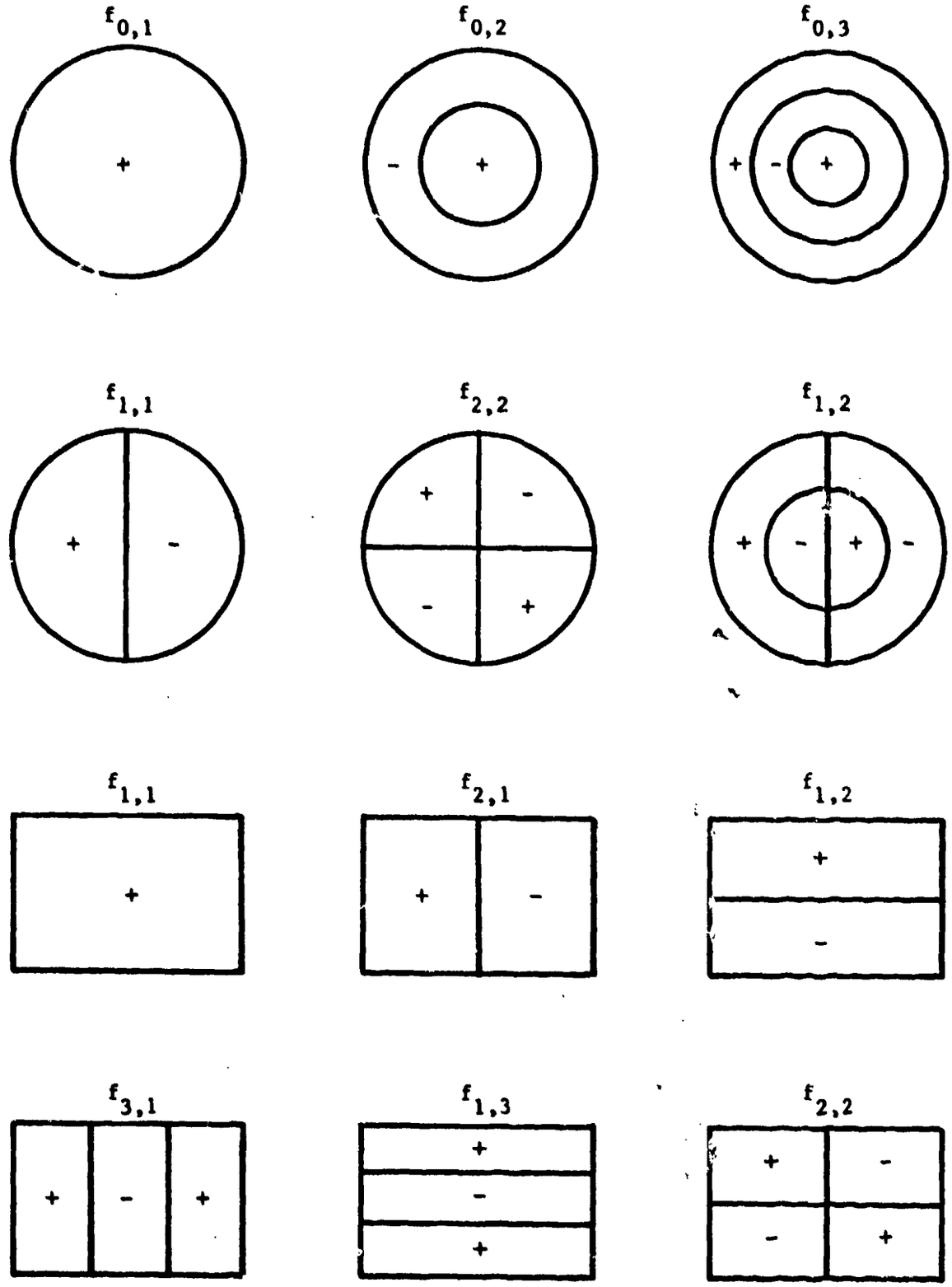

Figure 4. Modes of vibration for circular and rectangular plates. Patterns become progressively more comples as the mode increases. Higher modes are rarely seen because they attenuate very quickly.

$$\xi(x,y) = 0 \qquad \text{for } y = 0 \text{ and } b.$$
$$\xi(x,y)_{,y} = 0$$

The solution to equation (2) is

$$\xi = A\sin(s\pi x/a)\sin(t\pi y/b),$$

where s and t are integers. The frequencies are given by

$$f_{s,t} = \omega_{s,t}/2\pi$$

$$f_{s,t} = (h\pi/2)(s^2/a^2 + t^2/b^2)\{E/12\rho(1 - \sigma^2)\}^{\frac{1}{2}}. \qquad (5)$$

Since the tunnel beneath the Pisgah lava flow had a ceiling that could be approximated by a rectangle, the characteristic vibrations were found using equation (5). The following were the values needed;

Poisson's Ratio	$\sigma = 0.25$
Young's Modulus	$E = 2.33 \times 10^9$ nt/m^2
Density	$\rho = 2.20 \times 10^3$ kg/m^3
Length	$a = 100.0$ m
Width	$b = 10.0$ m
Thickness	$h = 2.5$ m.

The constants σ, a, b, and h were taken from Watkins *et. al.*. A standard value for vesicular basalt was assigned to E (Clark, 1966). Substituting all the above values into equation (5), and setting s and t equal to one, gives

$$f_{1,1} = (2.5\pi/2.0)(1/10^4 + 1/10^2)\{2.33 \times 10^9/12(2.20 \times 10^3)(1 - .25^2)\}^{\frac{1}{2}}$$

$$f_{1,1} = (3.91)(1.01 \times 10^{-2})(4.89 \times 10^2)$$

$$f_{1,1} = 19.3 \text{ hertz.}$$

Higher modes result in higher frequencies and as shown in Figure 4, more complicated patterns. Higher modes are often not found, since they tend

to dampen quickly. The above answer is the simplest characteristic vibration for a rectangle and it is very close to the 16 hertz signal associated with the Pisgah lava tunnel.

The information on the dimensions of the chimney formed by an underground nuclear explosion and on the rock type capping it was not exact enough to satisfactorily work the frequency problem. However, by making several different sets of assumptions for equation (4), the frequencies calculated usually came to be between 10 and 20 hertz. The field measurement was 12 hertz. The data for the Kana-a lava tunnel were insufficient to even make this kind of approximation.

In the previous section, we proved that neither axial or circumferential cavity waves could explain the resonance found over a few underground chambers. In this section, we have shown that the frequencies of flexural waves agree well with those measured in the field. This implies that flexural waves may be of value in detecting certain types of caves. The special characteristic needed for their generation is a thin roof with a large surface area. This feature would explain why resonance has not been found by Godson and Watkins, Rechtien and Stewart, and Stilke for relatively deep caves. Presently this is an unproven, but promising theory. To conclusively prove that cavity resonance is due to flexural waves, it will take extensive field work in comparable areas, with special attention to cavity dimensions and the physical properties of the surrounding rock.

RAY TRACING

Cook found a decrease in the normalized amplitudes of waves recorded above brine cavities. He concluded that these anomalies were caused by a seismic "shadow" formed when the cavity acted as an obstacle to a portion of the up-coming reflections. Watkins *et. al.* had a similar amplitude decrease above the Kana-a lava tunnel and over the U4B underground nuclear test site. At this location they also recorded delays in arrival times. Apparent delay times were also seen over some Missouri caves investigated during this study. The first attempt to theoretically study this "shadow" phenomenon was with ray tracing.

Cavanaugh (1973) had developed an efficient computer procedure for the iterative tracing of rays through volumes containing complicated boundaries. This differed from the usual methods by being able to handle high-powered polynomial surfaces as easily as simple surfaces and by using the three-dimensional form of Snell's Law. This is a vector equation and is written

$$(1/V_0)(\bar{I} \times \bar{N}) = (1/V_1)(\bar{R} \times \bar{N}), \qquad (1)$$

where

V_0 = velocity of the medium containing the incident ray,

V_1 = velocity of the medium containing the refracted ray,

$\bar{I}$ = unit incident ray vector,

$\bar{R}$ = unit refracted ray vector, and

$\bar{N}$ = unit vector normal to the interface between the two media.

Figure 5 shows a generalized boundary intersected by the incident vector $\bar{I}$. The plane of refraction is defined by $\bar{I} \times \bar{N}$. When the magnitudes of the cross-products in (1) are calculated, the result is the familiar expression of Snell's Law in two-dimensions.

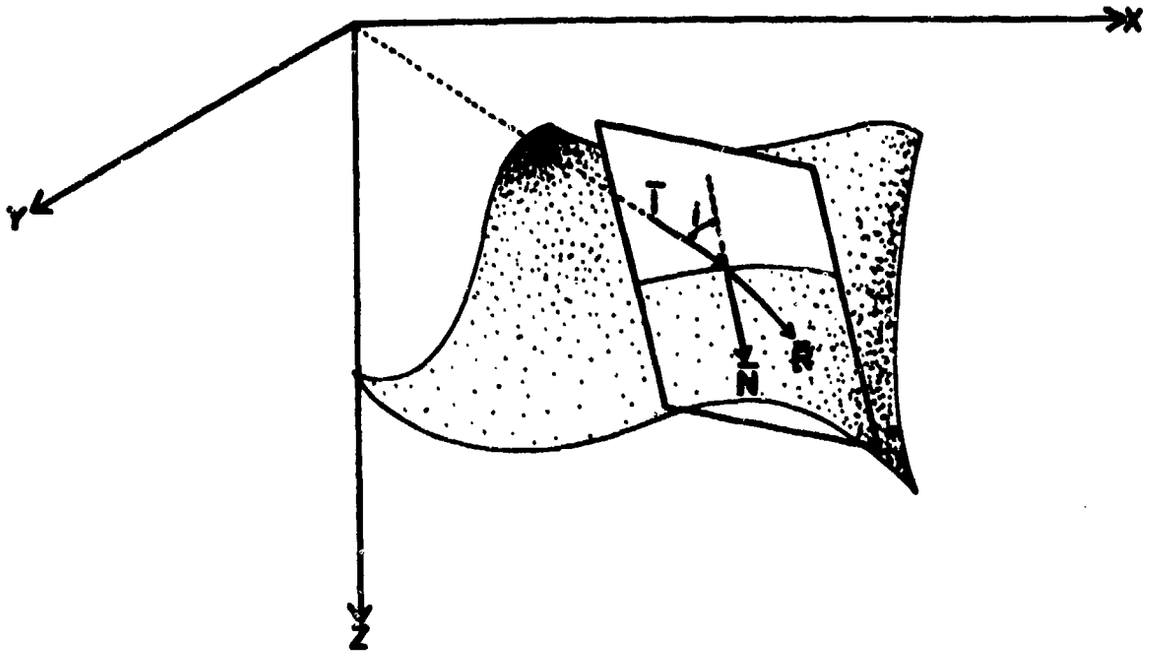

Figure 5. The plane of refraction and reflection as defined by $\bar{I} \times \bar{N}$.

Using this vector equation, Stravroudis (1972) derived the following formula for the unit refracted vector;

$$\bar{R} = \Gamma\bar{N} + \mu\bar{I}$$

where

$$\mu = V_1/V_0$$

$$\Gamma = -\mu\cos(i) + \{1 - \mu^2\sin^2(i)\}^{\frac{1}{2}}.$$

When reflection is considered as a special case of reflection, it is seen that $\mu=1$ and $\Gamma=-\cos(i)$. This implies

$$\bar{r} = -2\cos(i)\bar{N} + \bar{I},$$

where $\bar{r}$ is the unit reflected vector. By defining the plane of refraction and reflection at every point of intersection and by using the equations for $\bar{R}$ and $\bar{r}$, it is possible to mathematically construct a ray's path through almost any volume.

Most natural cavities are smaller than the wavelengths of waves that propagate through the earth's crust. Ray tracing cannot be used for this case because of dispersion. However, it was hoped that it could be applicable to underground chambers with extremely large dimensions, such as some brine cavities.

In order to produce the most realistic results, modifications were made to the basic ray tracing program. Boundary phase changes were added and amplitudes were adjusted at each point of reflection and refraction so as to agree with the division of energy predicted by the Zoeppritz equations. However, this approach was soon abandoned. The exponential increase in rays due to phase conversions for both refractions and reflections created time consuming computer runs, even for the simplest models. Ray tracing also could not predict interference patterns, diffractions, or the form of any resulting surface waves. What was being

done was an attempt to take some of the simplified properties of waves (Snell's Law, Zoeppritz equations, and phase changes) and use them to model in detail, a very complicated form of wave propagation. It became clear that this type of modelling could only be done successfully if you went back to the source of these properties—the wave equation.

WAVE SCATTER

Because most caves are smaller than the lengths of seismic waves, it is not possible for them to be opaque, even with respect to a pure shear wave. For a large cavity, energy will be transferred to the leeward side by various surface waves and by diffraction. Therefore, instead of a cave having a seismic "shadow", it will probably have an area of complex "turbulence", which could be compared to that found behind a pier pile after an ocean wave has passed. This "turbulence" is formed by a combination of reflected, refracted, and diffracted waves, and it is called wave scatter. To solve scatter problems, it is necessary to use the wave equation, that can be solved by either analytical or numerical methods.

Analytical Solutions

Ying and Truel (1955) worked the problem of a plane P-wave moving in an infinite, elastic solid, and incident upon a spherical obstacle. They considered three types of spheres; void, elastic, and rigid. For the last two obstacles, three separate waves were derived. They were the unimpeded incident wave, the scatter wave formed at the obstacles surface, and the wave generated within the sphere. The void would be analogous to an air-filled cave, which unlike the rigid and elastic spheres, would not form an internal wave.

Ying and Truell completed all equations of motion and set all boundary conditions in spherical coordinates. They also restricted particle motion to the two-dimensional $\rho\theta$-plane. The scalar potentials for the three separate obstacles became expressed in Spherical Bessel Functions, and these were used to calculate the scattering cross-sections

for each case. The components of the displacement vector were not found, but they were obtainable from the equations provided.

White (1958) did a similar problem for a cylindrical scatterer imbedded in an infinite, elastic medium. The obstacles studied were elastic, void, and fluid-filled cylinders. The second and third could be used as models for air-filled caves and ones containing water or mud. The incident plane P- and S-wave possessed a single frequency and could strike the cylinder at any angle of incidence. The vector potential was not converted to a scalar by limiting particle motion to a single plane. The problem was solved in three-dimensions, with the scalar and vector potentials being expressed in terms of Bessel and Hankel Functions. This derivation also demonstrated that an incident P- or S-wave will result in scattered waves of both types. This is referred to as mode conversion.

The derivations by White and by Ying and Truell provide much information concerning the problem of scatter, but both have serious limitations, which restrict their usefulness for the theoretical study of cave detection. In seismology, ground motion is measured at the earth's surface, which indicates that for the cave problem there are two important boundaries; the surface of the cavity and the surface of the ground. Neither of the above derivations considered a second planar boundary. To have included such an interface, would have created extreme difficulties with boundary conditions, since a plane that does not go through the origin is not easily expressed in cylindrical or spherical coordinates. Without a plane boundary, the interaction between the scattered wave and the surface of the ground cannot be accurately known. The second drawback is that the cavities must mirror the coordinate system used. This results in targets of very simple shapes. Again, this is dictated by the fact

that uncomplicated boundary conditions are needed to solve the analytical problem efficiently and accurately. These difficulties can be avoided by solving the scatter problem numerically.

Numerical Solutions

Both the finite element and the finite difference methods may be employed to describe the behavior of scattered waves. These two numerical procedures have some common properties. Except for trivial cases, each requires the use of computers. This has restricted their application in the past. Both techniques represent the geological profile with a set of points and both use the basic form of the wave equation;

$$\rho\overline{U}_{,tt} = (\lambda + \mu)\nabla\Theta + \mu\nabla^2\overline{U}.$$

These properties allow the problem to be solved in the rectangular coordinate system and they permit very irregular cavities without difficulties with boundary conditions.

With the finite element method, each point represents a "lumped" mass, and every pair of points is assigned elastic properties that are defined by the types of rocks encountered and the boundary locations. To generate wave motion through this maze of mathematical weights and springs, the second ordered differential wave equation is stated in terms of Hook's Law. A large group of simultaneous equations is formed when the values at the points are substituted into the modified wave formula. These can be solved at set increments of time by the Runge-Kutte algorithm. Each set of answers gives the positions of the model points in that time frame and the sum of these positions over a length of time defines the wave motion.

When using the finite difference procedure, the points of the model must be spaced at regular intervals. The values assigned to each point

depend on the density and the elastic moduli of the material surrounding that point. The only change in the wave equation is the replacement of the differentials by difference approximations. These formulae are in a form that can be easily programmed. The motion is found by iteration, where the movement of a point is directly dependent on the movement of that point and the surrounding points in the previous time increments. I have chosen to work with this method because it is relatively easy to program and it is extensively discussed in the literature.

There are several finite difference methods used to define wave motion. The first one to be applied to the problem of scatter was developed by Claerbout (1970). He devised a good one-dimensional approximation to the two dimensional wave problem. This is a very attractive feature in that it saves large amounts of computer storage space. This is usually the biggest problem encountered with finite difference methods.

Claerbout reformulated the wave equation in terms of pressure so that

$$\nabla^2 P = (1/C^2)P_{,tt} \tag{1}$$

where

$$C = (\kappa/\rho)^{\frac{1}{2}}$$

$$\kappa = \lambda + (2/3)\mu.$$

The term κ stands for incompressibility. The behavior of this pressure wave is identical to that of the P-wave. The solution to equation (1) in two-dimensions is

$$P = P_0 \exp(imz + ikx - i\omega t).$$

For a plane wave traveling down the z-axis, this becomes

$$P = P_0 \exp(imz - i\omega t).$$

The transmitted and the reflected waves together form a more complete

solution to equation (1);

$$P = P^{+}(x,z)\exp(imz) + P^{-}(x,z)\exp(-imz)\exp(-i\omega t).$$

P^{+} designates the transmitted wave and P^{-} the reflected wave. Note that both are now functions of location. If they do not vary rapidly, more computer space may be saved by using a coarse grid for the model profile.

The transmitted wave is separated from the reflected wave and numerical equations are developed to describe its behavior. These are solved iteratively with a row-by-row process that uses the left and right boundary conditions and the motion found on the previous two rows. In this way the wave patterns are developed over the entire velocity model. The wave amplitude values at each model point can then be used to generate the reflected waves by a similar row-by-row difference procedure.

Figure 6 and Figure 7 were plotted using the procedure for transmitted waves. Both patterns are formed by a P-wave moving from the bottom to the top of the illustrations. The scatterer represents a flat-floored chamber filled with mud. In Figure 6, the wavelengths are much smaller than the dimensions of the cavity. The wave patterns conform quite well with ray theory and the focusing of this mud lens is clearly shown. In Figure 7, the radius of the cave is smaller than the length of the wave and diffractions are shown to be an important feature. A time delay along the wave front is also present.

Even though these two figures illustrate refraction, diffraction, and interference patterns, there is a great deal of information that has been lost. In the Claerbout method, shear waves are neglected. This prevents the formation of mode converted waves by the scatterer. These S-waves would be an important factor in the interference patterns found above a cavity. Also, without S-waves, an accurate description of ground

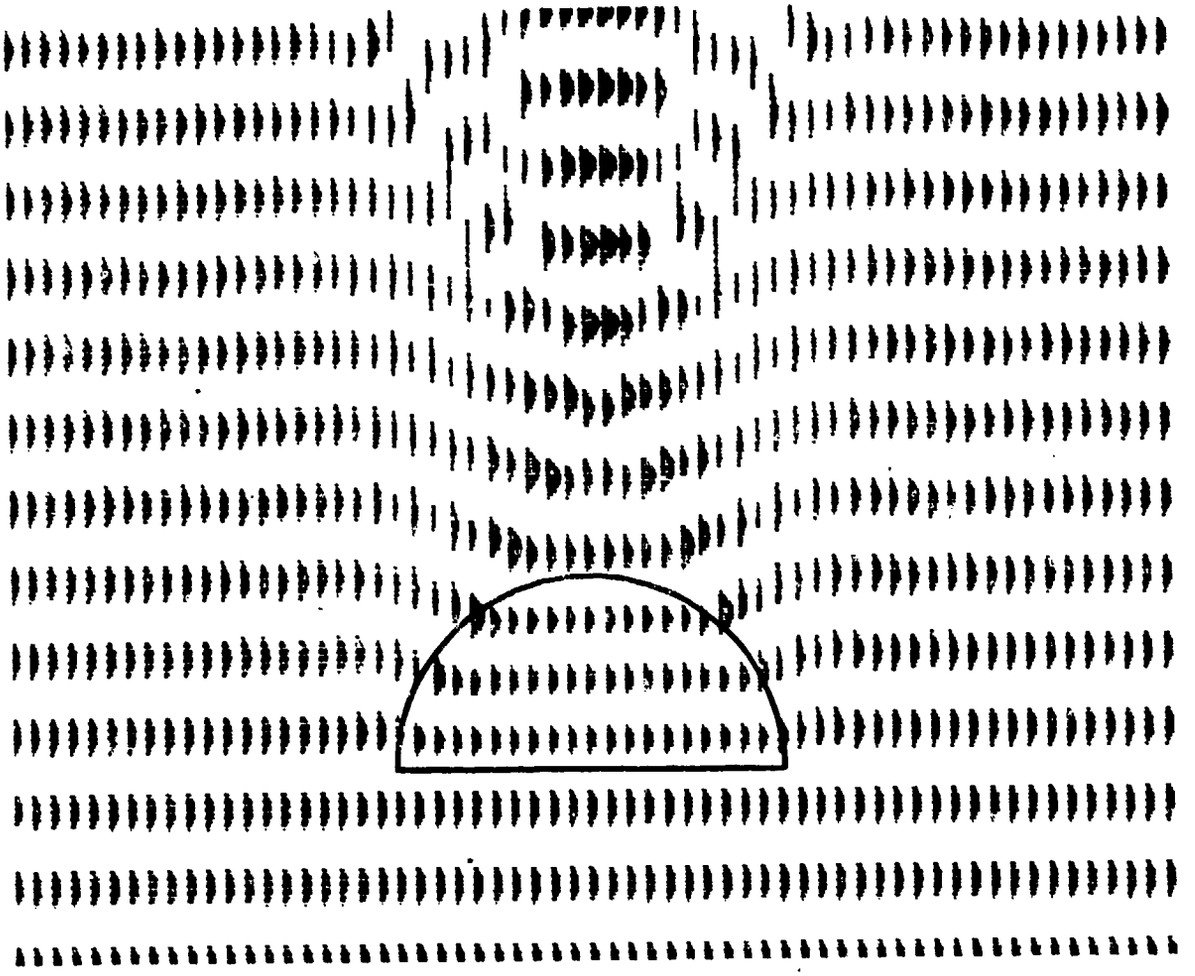

Figure 6. Wave pattern when cavity's radius is greater than wavelength.

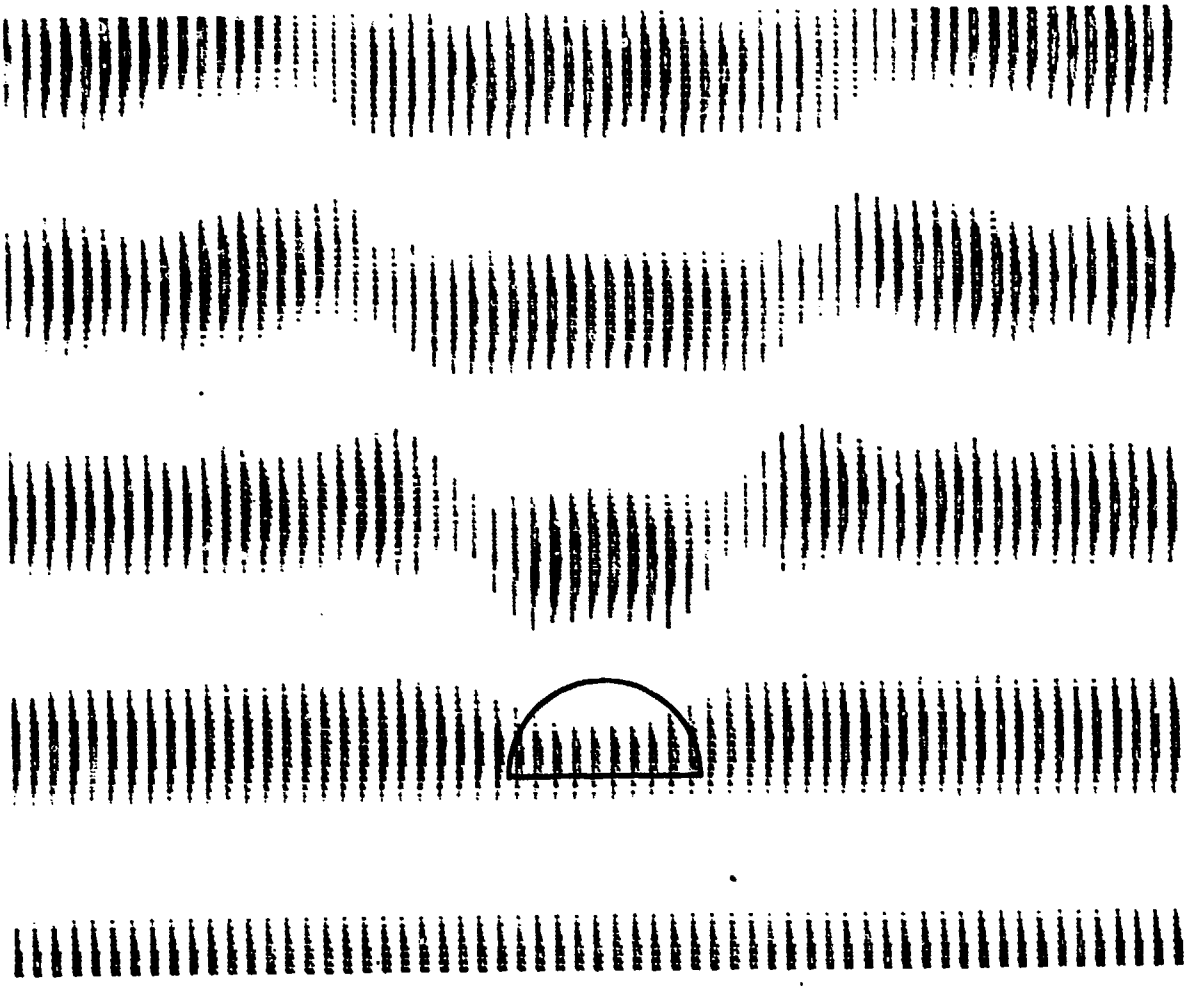

Figure 7. Wave pattern when radius of cavity is less than wavelength.

motion is impossible. Another difficulty with the Claerbout method, is that due to the approximations made, the amplitudes of the waves become unstable as the wave deviates from the vertical. This is serious since voids often develop large-angle diffracted waves. Even with the large computer costs, the best way to study scatter is with a complete finite difference technique.

As a continuation of the research sponsored by the Army, the Ph.D. dissertation to be completed by Cavanaugh will be on the use of finite difference for the development of synthetic seismograms above air-, water-, and mud-filled cavities. The objectives of this computer modelling will be: (1) to obtain a better understanding of the "turbulence" created by a wave sweeping past a cavity; (2) to find if it is possible to delineate the shape, size, and depth of a cavity by the scatter that it causes; (3) to determine how to enhance the seismic signature of a cavity; and (4) to find what combination of size and depth will make the disturbance too insignificant to be recognized on a seismogram.

CONCLUSIONS

Biot's work demonstrated the existence of cylindrical surface waves, but the manner of their propagation makes them unusable for the detection of cavities. Even if these waves were recorded above a shallow tunnel, their velocity and particle motion would make them indistinguishable from the Rayleigh wave. For deep tunnels, they would not be noticed because of their rapid attenuation. In addition, the axial surface wave is a travelling wave and cannot be used to explain resonance. It was thought that circumferential surface waves on a cylinder could explain these oscillations, but they cannot be shown to exist theoretically. The long-lived, periodic vibrations measured above some cavities appear to be due to flexural waves. These can only be formed under the special condtion that the roof of the cavity behaves as a vibrating plate, thus restricting their occurrence to extremely shallow caves.

For caves that have substantial roofs, the anomalies of amplitudes and/or arrival times that are occasionally detected in a seismic "shadow" zone, may be a possible means of delineation. This "shadow" is likely a region of "turbulence" created by the cavity acting as a scatterer for an up-coming reflection. Wave scatter cannot be adequately investigated by analytical methods, because of the necessity of using very simple boundary conditions. The inability to complete the problem exactly in an infinite half-space makes it impossible to predict the interaction of the scattered wave with a plane surface. Claerbout's procedure, which is an approximation to the finite difference method, can be used for a model containing many interfaces with complex shapes, but its solutions can become unstable and the important behavior of shear waves is neglected. To obtain the best

mathematical description of cavity wave scatter, it will be necessary to use the complete finite difference method. This is presently being done as an extension to the work completed with the support of the Army.

In summary, the following theoretical approaches have been explored in this study:

1. Resonance;
   a) void cavities in infinite solids (intrinsic cavity resonance),
   b) void cavities in infinite half-spaces (resonance caused by the interaction between cavity and land surface),
   c) axial cavity surface waves observable at land surface,
   d) circumferential cavity surface waves observable at the land surface,
   e) the cavity roof acting as a vibrating mebrane, and
   f) the cavity roof acting as a vibrating thin plate.
2. Scattering;
   a) analysis by ray tracing using Snell's Law in three-dimensions and
   b) analysis by finite difference approximation to the wave equation.

Only the thin plate model and the finite difference approach seem to hold promise. The thin plate model would apply only to cavities very near the surface. For deeper caves, the finite difference approximation for wave scatter offers the best possibility of producing a general method of detection. This has yet to be fully developed.

SECTION TWO

EXPERIMENTAL STUDIES

ON CAVITY DETECTION BY SEISMOLOGY

INTRODUCTION

The experimental research conducted under this Grant was directed towards the development of a seismic field procedure for the detection and delineation of subterranean cavities. The basic underlying presumption of this study was that a resonance phenomenon is associated with voids when they are subjected to an induced seismic field. This presumption was based on experimental evidence reported by Watkins et al (1967), and by Godson and Watkins (1968), and on theoretical evidence presented by Stewart (1971).

To illustrate the resonance phenomenon associated with voids, a seismogram over a lava tunnel, as reported by Watkins et al, is reproduced in Figure 1. They reported that the high amplitude oscillations, as

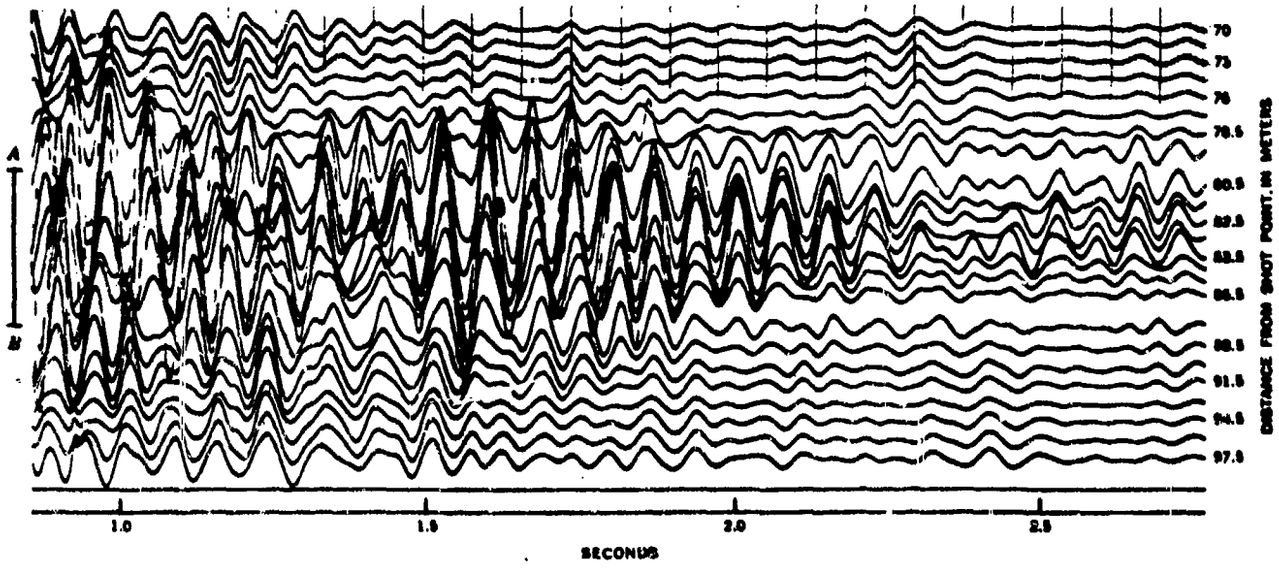

FIGURE 6.—Part of a seismogram recorded over a lava tunnel in the Pisgah lava flow, San Bernardino County, Calif. Note prominent in-phase cavity oscillations in center of seismogram. *AB* indicates the location and approximate width of the tunnel.

Figure 1. from Watkins et al (1967)

shown, were recorded most intensely directly over the cavity, and that this result was similar to the seismograms recorded over two other near-surface cavities that were studied. They noted that the dominant frequency is relative uniform with time, and that the in-phaseness of the oscillations was indicative of resonance.

Figure 1 in itself presents a very strong argument for cavity resonance, and based on this result the initial research effort was directed towards a more accurate definition of this phenomenon.

EXPERIMENTAL PROCEDURE

Test Sites The bulk of the seismic investigations were conducted over segments of Cathedral Caverns and Onondaga Cave, located approximately seven miles south of Leasburg, Missouri. Measurements were also taken at three other test sites over known cavities, cave systems, or suspected cave systems, but have yielded little results. In these areas the principal problem was the uncertainity of the siesmic traverse relative to the underground void, excessive depth of the cavity system, and the cavity size. Consequently, results will only be presented for the Cathedral-Onondaga areas.

A plan view of the Cathedral-Onondaga systems is shown in Figure 2. Seismic lines that shall be discussed in this report are shown in the figure as dark lines designated as T1, T2, and T3.

Traverse T2 is over a known, and accurately surveyed, cave passage. The trace of this passage above ground was determined by means of surveying. The passage in this segment of the tunnel is rather uniform in shape with a height of roughly 10 feet and a width of 51 feet. The roof is located approximately 162 feet below the surface.

Traverse T1 was seismically surveyed to detect a possible extension of the western segment of Cathedral Caverns. Traverse T3 was conducted in the vicinity of Onondaga Cave in an attempt to detect an extension of a water filled segment of the cave. Both T1 and T3 were traverses over previously unexplored areas.

During the course of the three years of this grant, and for two years prior to the initiation of this grant, these test sites were repeatedly investigated many times, with slight modifications of the traverse orientation,

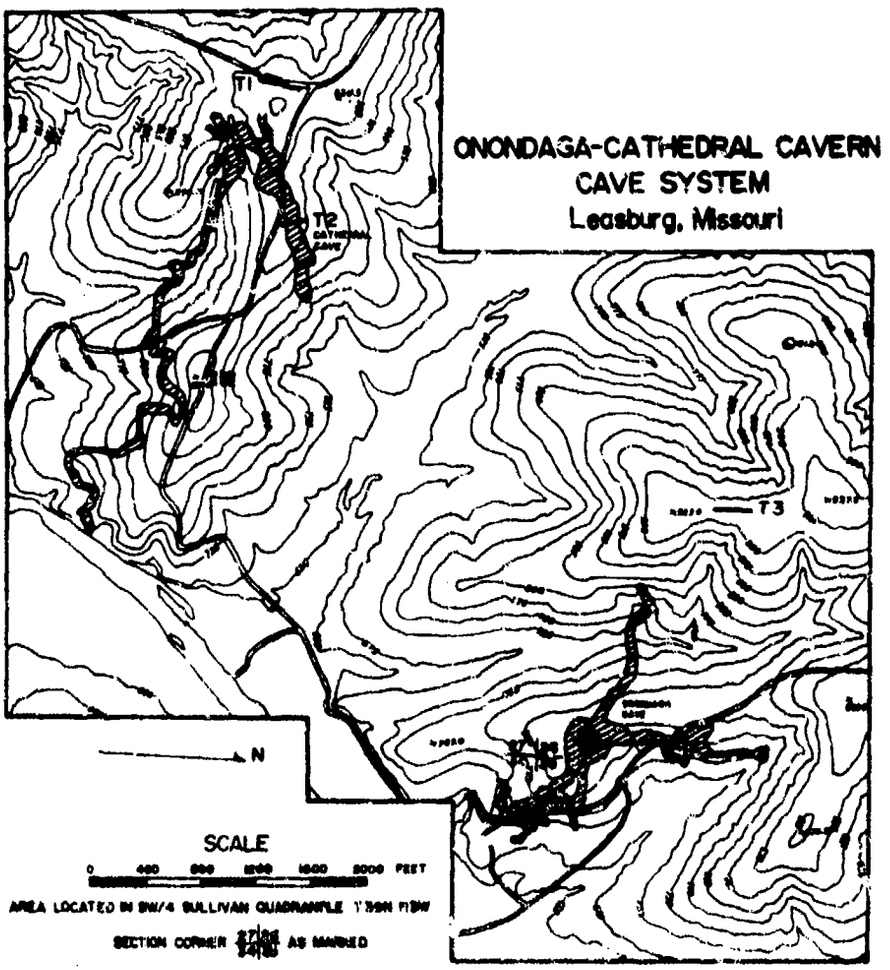
ONONDAGA-CATHEDRAL CAVERN
CAVE SYSTEM
Leasburg, Missouri
T1
T2
T3
N
SCALE
0 400 800 1600 2000 FEET

Figure 2.

improved instrumentation, or principally to test a reorientation of the research direction.

Instrumentation Ground velocity was measured with Sprengnether, Model S-6000, three-component, short period seismometers, and digital grade vertical and horizontal seismometers. The seismometer outputs were [illegible] through programmable gain amplifiers, processed through a 32 channel analog to digital converter and NOVA 800 Jumbo Computer, and permanently stored on a moving head Diablo cartridge disk system.

The data acquisition system and reduction system is described in Appendix A of this report. The acqusition system is housed in a seismic van as shown in Figure 3. The basic computer acquisition system as installed in the van is shown in Figure 4.

The frequency response of the seismic system is flat from 2 to 200 Hertz for the system using Sprengnether seismometers. Using the digital grade seismometers the response of the system is flat over the range of 8 to 200 Hertz.

In the results presented a chemical explosive was used as the energy source. Early investigations employed a mechanical vibrator. However the energy production of the instrument was far too low to be useful.

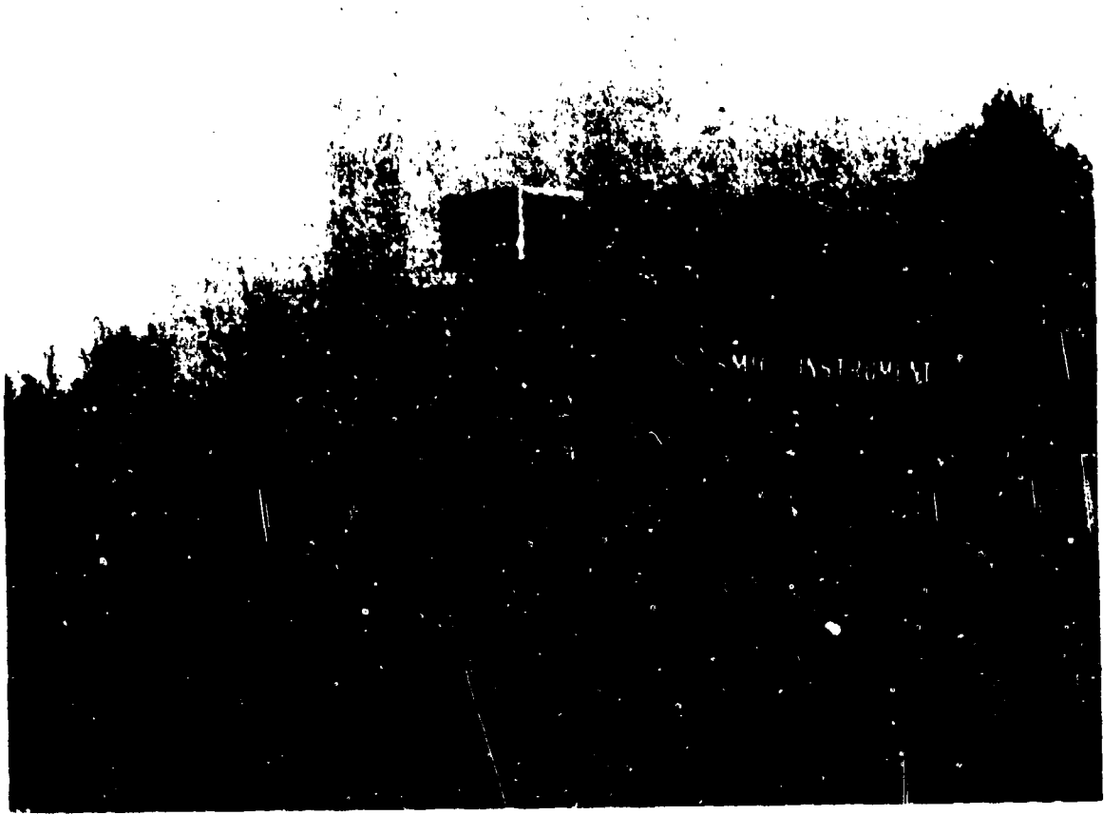

Figure 3. Seismic van.

Figure 4. Data Acquistion System

RESULTS

The cavity underlying Traverse T2 was chosen as the principal scattering object to be studied. This cavity exhibited mud-free walls, uniformity in shape and direction over a large portion of its length, and accurate spatial measurement control. Moreover, this roughly eliptic-cylindrical void was not too large, nor too small, and was located at an interesting depth of 162 feet below the surface. Cavities of this size and depth have hitherto been opaque to geophysical probes.

The principal results of this investigation were obtained over this tunnel, after many, many trials. These results are shown in Figure 5 which presents portions of the three-component measurements along Traverse T2. The measurements shown were taken at 10 foot intervals along a line oriented at a right angle to the cavity axis. Seismometer #6 was located directly over the center of the cavity. The shot point was 50 feet from Station 1.

From the volume of data taken in the near proximity of Traverse T2, many different seismic indications of the presence of a cavity were discovered. Some of these indicators are discussed in Rechtien and Stewart (1975), which include direct scattered P and S wave energy from the cavity roof, and the predominance of horizontal motion in planes parallel to the tangent planes to the cavity at late arrival times. These results still stand. However the analysis of early arrival times is subject to considerable error, particularly in this area where the topography is rugged and weathering depths and velocity vary considerable over short distances.

On the other hand, the horizontal motion in planes parallel to the cavity boundary have been consistently observed, often with energies far exceeding the SH wave energy proceeding from the source. In addition a reflected Love wave from cavities has been observed, but not consistently. The only type of seismic event that has been measured consistently is illustrated in Figure 5. But before describing these results it might be worth stating that over all air filled cavities with mud free walls that were investigated, never was a record obtained that exhibited the "resonance" signature of Figure 1, as reported by Watkins et al. However the cavities in the area of T2, and at other locations, were considerably deeper than those reported be Watkins et al. And perhaps the shallowness of the cavity that they investigated is a significant factor to their results.

Figure 5 presents the results of three-component ground velocities from 400 to 700 milli-seconds. Earlier data is predominated by surface wave energy which shows normal transmission behavior. Later data shows random, scattered phase arrivals and is of little interest.

The data as shown has been processed through a digital band pass filter after the data was windowed by a function which allowed suppression of the data below 350 milli-seconds and above 1,700 milli-seconds. The windowing was performed to suppress the effect of the high energy surface waves on the band pass filtering process. The inclusion of the high frequency data, above 35 Hertz, seriously distorts the data. Although the basic pattern illustrated in Figure 5 is there, it is not at all obvious to the naked eye.

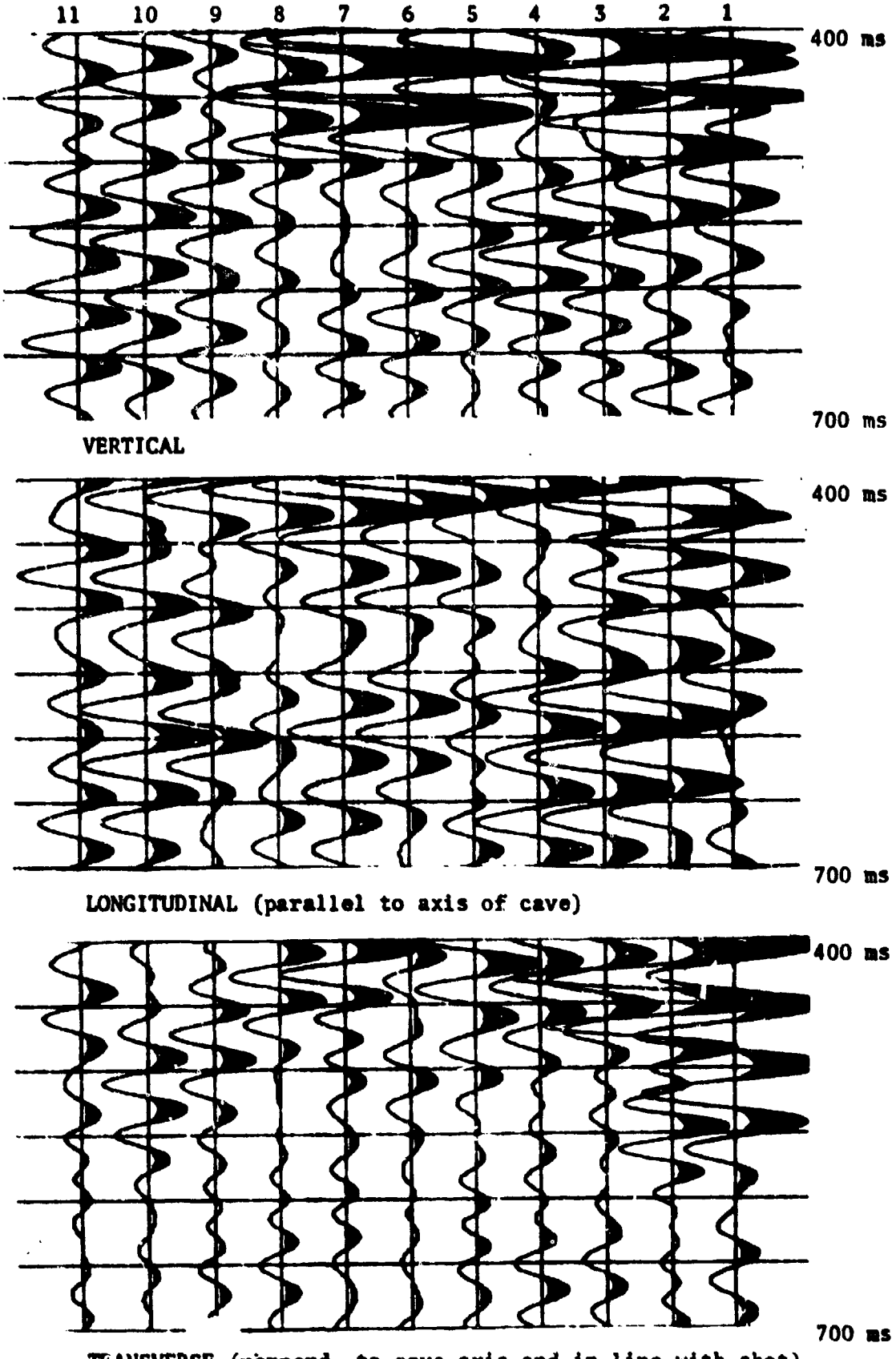

Figure 5. Three component seismographs, traverse T2, 17-35 Hertz, windowed 350-1,000 ms, spacing 10 feet, shot 50 feet to the right.

The first indication of a cavity is shown on the Vertical data by events that are concave upward in the central portion (500-600 ms) of the seismogram. Note the negative (un-shaded) event which begins at Station 1 at 550+ ms and ends at Station 11 at the same time and dips to 580+ ms at Station 6. The following negative event parallels this some 85 ms later, and the negative event preceding shows the same concavity upwards on the flanks of the cavity, but in fact it is convex downward over the central portion of the void at Stations 6 and 7. A dead spot results beneath this convexity where the positive (shaded) energy diminishes to near zero through destructive interference. The downward convexity of the positive event directly above this dead spot is even more pronounced. Also note the high energy events directly above this shadow zone between Stations 5 through 8 between 425 to 475 ms. This high energy event shows no phase relationship with the traces on either side.

On the longitudinal data it is obvious that Stations 5 and 8 are points of phase reversals across the records between 450 to 600 ms. At 640 ms Stations 1 through 4 and 9 through 11 have positive (shaded) phase, whereas Stations 6 and 7 are reversed in phase, and Stations 5 and 8 are somewhat nulled. This behavior can also be followed at earlier times to 450 ms.

The Transverse data show little or nothing in this record interval. If anything it shows a diminishing of wave energy in the central portion of the traverse.

Particle velocity hodograms for Stations 3, 6, and 9 for the seismic interval of 520 to 600 milliseconds are shown in Figure 6. These hodograms are typical of the entire traverse and seem to imply that the vertical and longitudinal motions are independent. This conclusion is not too surprising since the Wave Equation in a cylindrical coordinate system naturally separates motion in the r-θ plane to be independent of axial motion. Consequently the results are more meaningful as viewed from the time traces themselves.

The identification of a diagnostic event, or sequence of events, as given in Figure 5, is the principal result of this study. Although the mechanism that results in this cavity signature on a seismogram has not been identified, it seems probable that it is a surface wave phenomenon, either associated with cavity interference with a deep penetrating surface wave travelling away from the source, or from surface waves associated with the cavity itself and generated by mode conversion from waves reflected from deep horizons, or from entrapment of passing surface wave energy.

The data of Figure 7 sheds considerable light on this question, and very clearly supports the deep penetrating surface wave interference line of thinking. This seismogram was obtained over a segment of Cathedral Caverns in the vicinity of Traverse T1. Fifteen seismic stations are shown and one three-component measurement which was taken at a point near Station 1. This record has not been filtered, and in fact the frequency spectra of these traces are shown in Figure [illegible].

This particular shot was not in-line with the traverse.

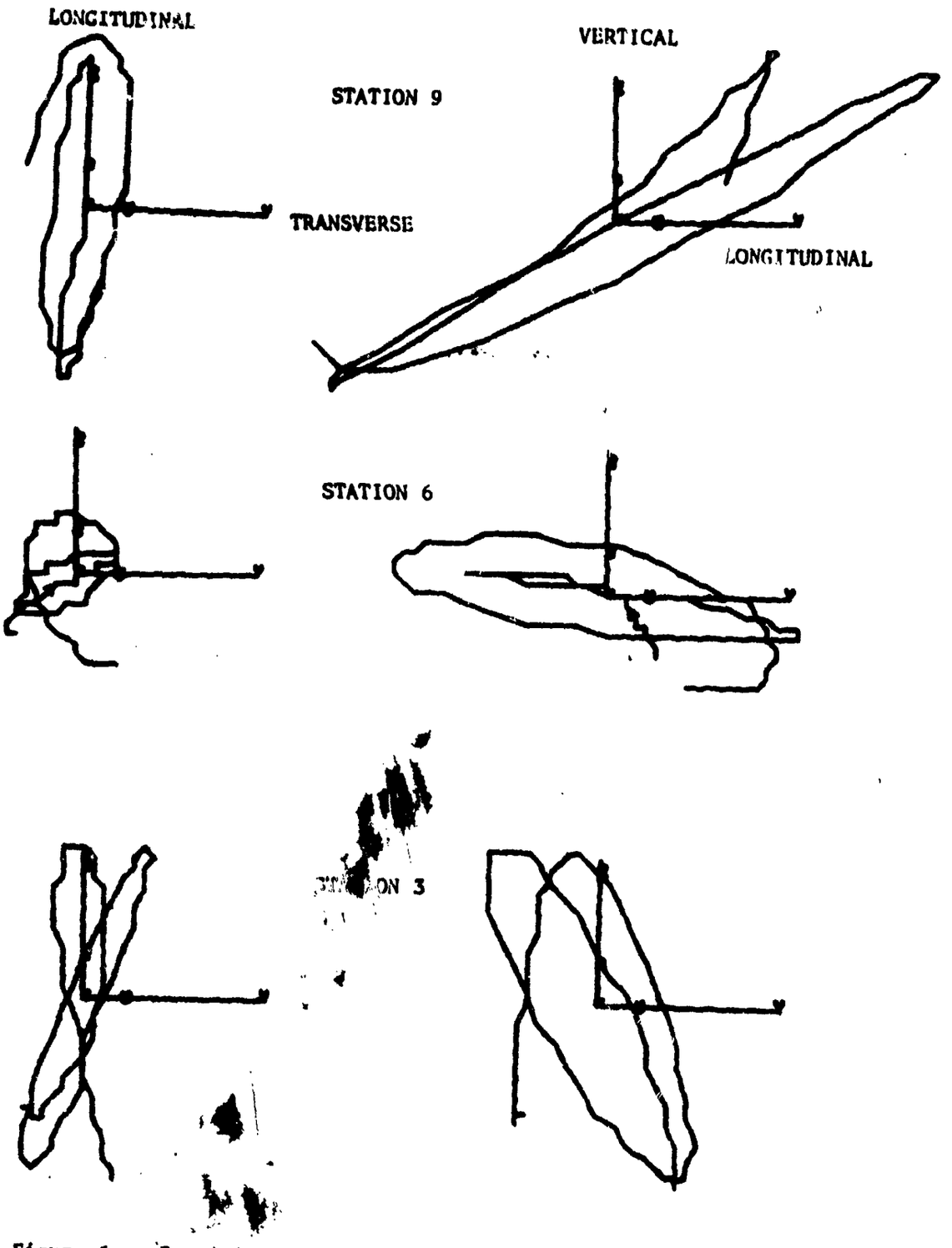

Figure 6. Particle velocity hodograms for Stations 3, 6, and 9.

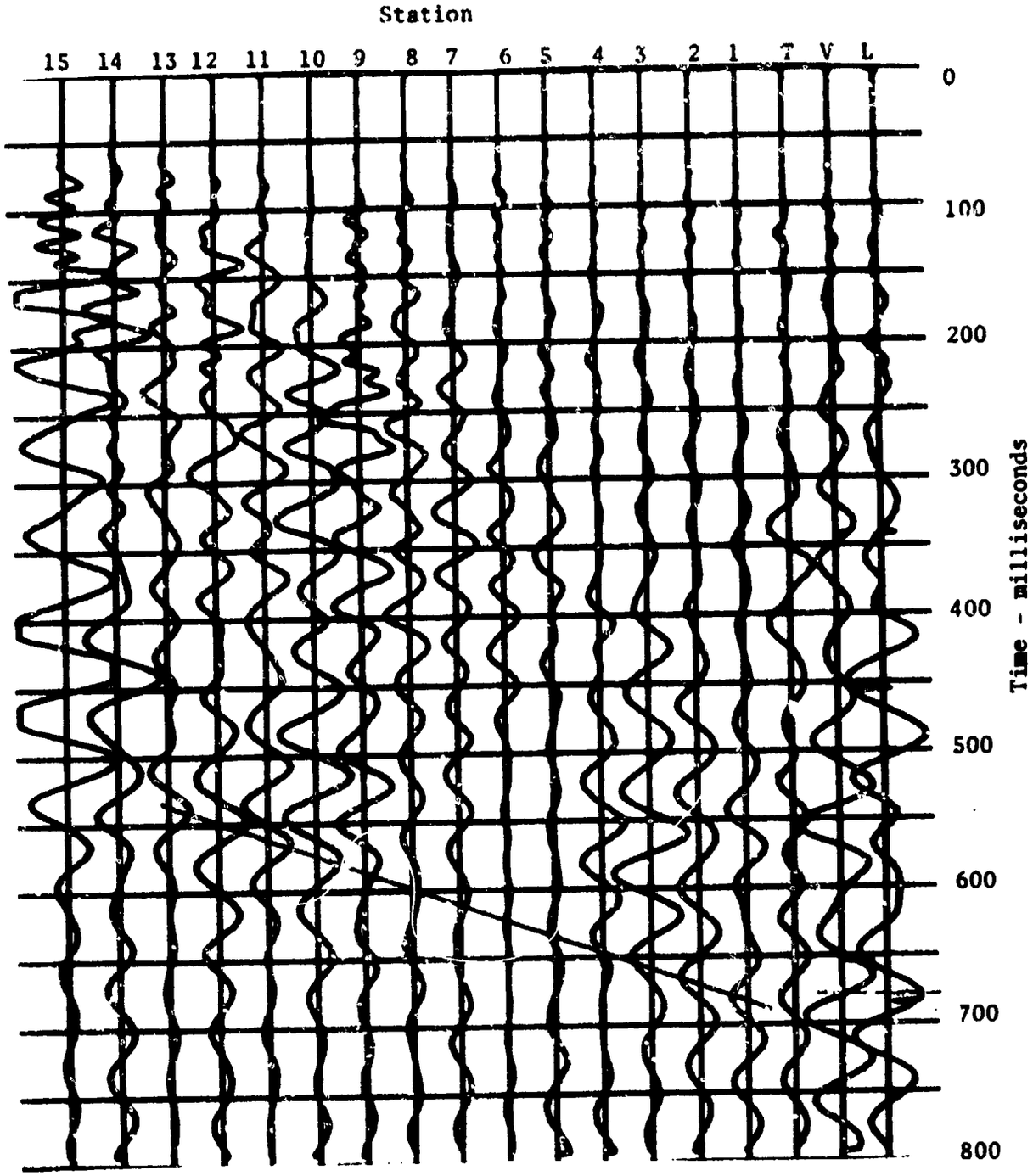

Figure 7. Seismogram of vertical motion, Shot 1, line 11.

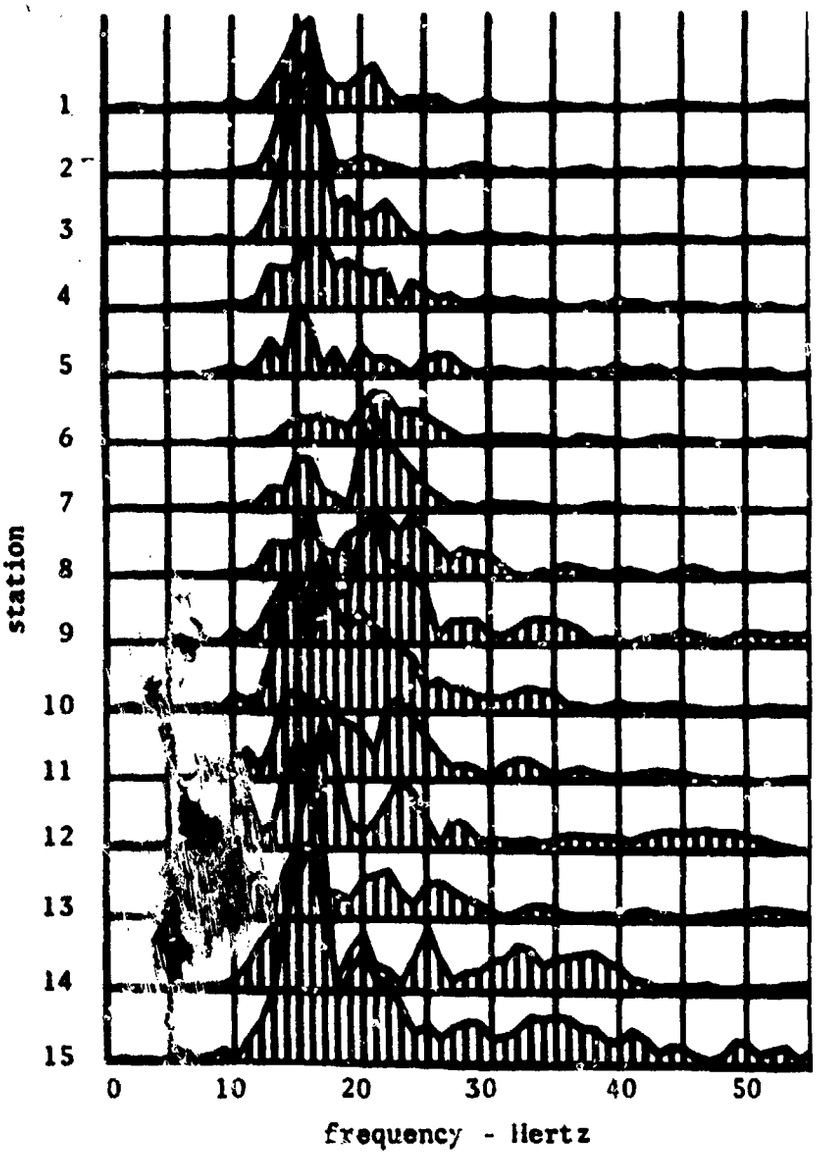

Figure 8. Frequency Spectra, Shot 1, Line 11.

In reference to Figure 7, a dead spot is shown in the vicinity of Station 6 around 600 ms. Station 6 overlies a cavity of approximately the same size and depth of burial as that of Traverse T2. It seems presumptuous to identify a wave on this record by drawing a straight line, but for the purpose of focusing on a particular segment of the record a straight line has been drawn. This straight line goes through points of common phase on both sides of Station 6, although the data to one side of Station 6 is 180 degrees out of phase with that on the other side. If one would calculate velocities from a delta-t - delta-x analysis, an extremely slow velocity, in the range of 700 feet per second would be obtained. Yet, the three-dimensional counterpart of the 680 ms wiggle on trace one clearly exhibits the 90 degree vertical-horizontal phase shift of a Rayleigh wave. Moreover, the data is clearly indicative of waves travelling to the right, away from the source, as they should. It appears, therefore, that the dead spot, at least in this instance, is due to the interference of the cavity with a passing, deep penetrating surface wave. It is hard, however, to account for such a slow speed. Moreover, the concave and convex curvatures and high energy events above the void, which were clearly evident on the data of Traverse 2, are not present in this record.

In reference to Figure 8, the surface wave energy centered at approximately 16 Hertz is clearly diminished over the cavity. This result was common to the data of Traverse 2 as well as to all the data taken over known cavities.

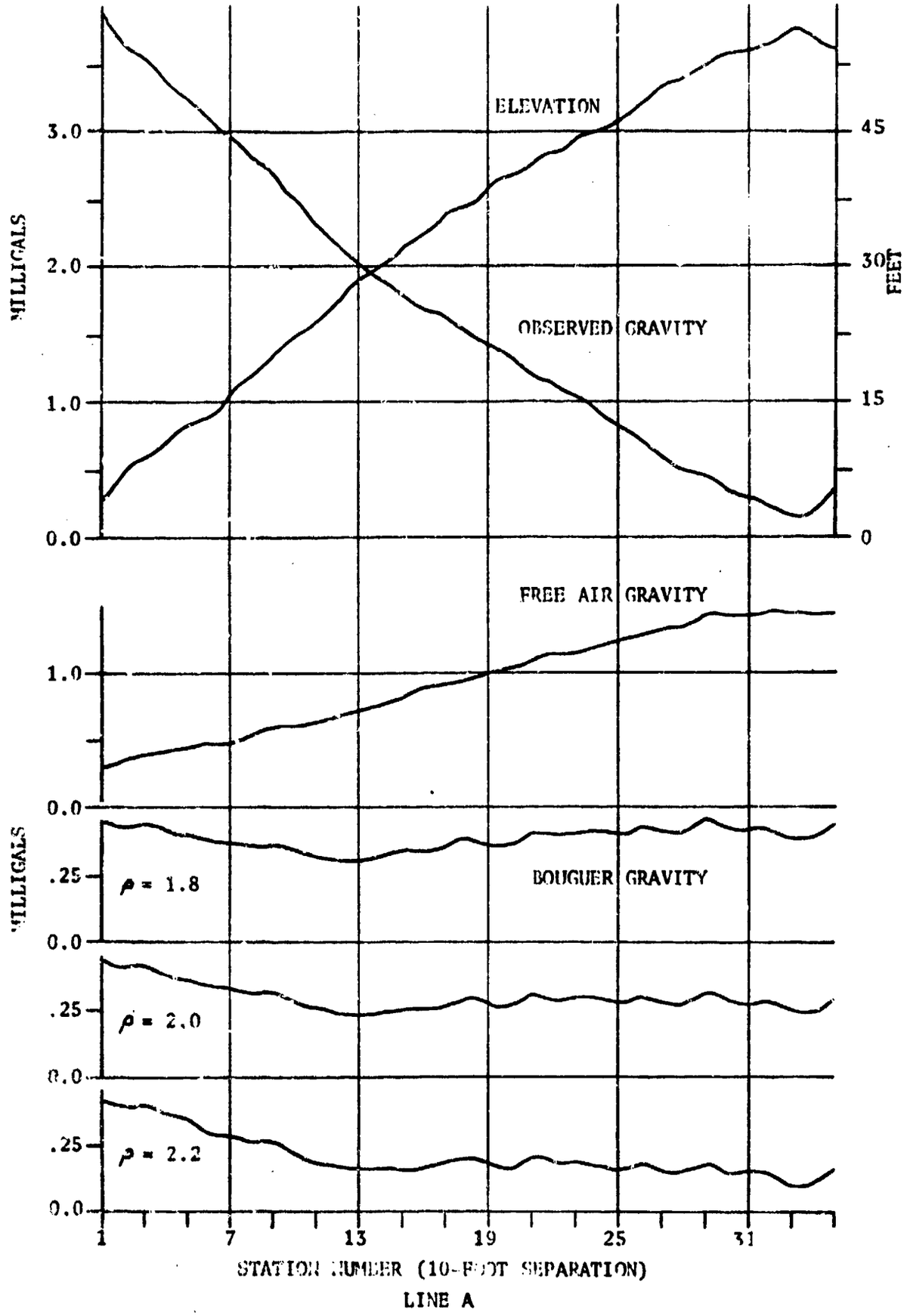

Figure 9. Gravity profile over Traverse T2

Before leaving Traverse 2 it is instructive to consider the gravity anomaly over this traverse. This data is shown in Figure 9, with Gravity Station 21 corresponding to Seismic Station 1, and Gravity Station 11 corresponding to Seismic Station 11. There is a faint gravity anomaly in the vicinity of Gravity Station 13. This anomaly is hardly noticeable in the observed or free-air gravity profile, and in fact one wonders if the anomaly is not just a correction effect. Regardless, gravity hardly seems like a feasible tool for cavity detection of this size and depth. These measurements were taken with a Worden Gravity Meter.

The elevation of the traverse illustrated in this figure shows the typical problem encountered in the search for cavities; they are usually found beneath steep slopes of hillsides. This fact creates serious problems in the interpretation of the results.

Figure 10 shows the seismic results along Traverse T1. This data was actually acquired prior to the initiation of this grant over an area of an unexplored region of Cathedral Caverns. Because of the numerous indications of cavities along this traverse, this area was chosen to test a series of broadside shots in an effort to obtain three-dimensional coverage of the subsurface using CDP techniques.

In Figure 10, surface waves dominate the record down to about 700 ms in both the forward and reverse shots. On the North shot data a dead spot first occurs near Station 7 at around 250 ms, and again in the vicinity of Station 12 at 500 ms, and at Station 25 at 700 ms. These all appear to be disruptions of the passing surface waves. Station 25 on the South shot also appears to be in the

neighborhood of a dead spot at about 600 ms, and Station 21 at 250 ms and 1050 ms. One can also see many areas of convex and concave curvature in the records. Two clear examples can be seen on the South shot; the convex curvature between stations 19 and 27 at about 570 ms, and the concave curvature underlying the dead spot at 700 ms; then again the convexity at 1000 ms between Stations 17 and 24, and the underlying concavity at 1100 ms. It is very clear that at least the tops of these dead spots are the terminal end of a passing surface wave. These data are much like the data of Traverse 2, except for the high energy, inphase events directly over the cavity. Recent exploration of Cathedral Caverns has resulted in a subterranean passage in this area, although its precise location is not known.

Very strong phase reversals on traces 7 and 14 in the neighborhood of 1000 ms on the North shot data can be seen. This reversal can also be observed at Station 8 at 800 ms on the South shot data. This behavior is similar to the results of Figure 7. The rather strong reverberations in this region of the North record and the reverberations between stations 7 and 11 on the South shot is somewhat indicative of the resonance reported by Watkins et al. There are no known cavities in this region. However, a gravity survey over this traverse was performed, and the results are shown in Figure 11. The gravity and seismic stations in this case coincide, and the data show a gravity low both over the area of reverberation near Station 9 and near Station 21. The question, "Why the reverberation?" arises. A cavity signature meets all the criteria near Station 21. But what is happening near Station 9?

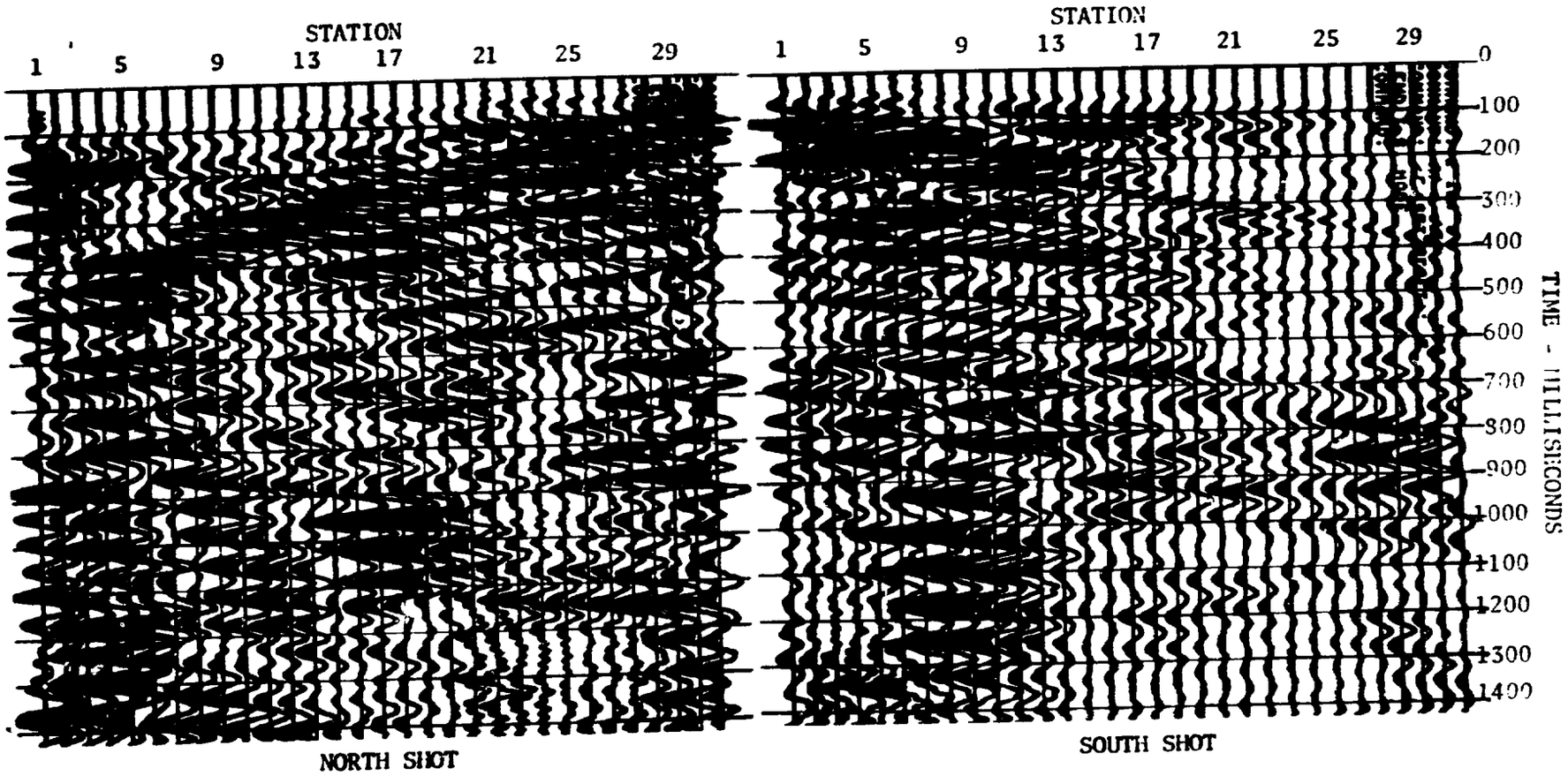

Figure 10. Forward and reverse shots along Traverse T1. Station spacing at 10 foot intervals, and the shot points are 100 feet from the end of the line.

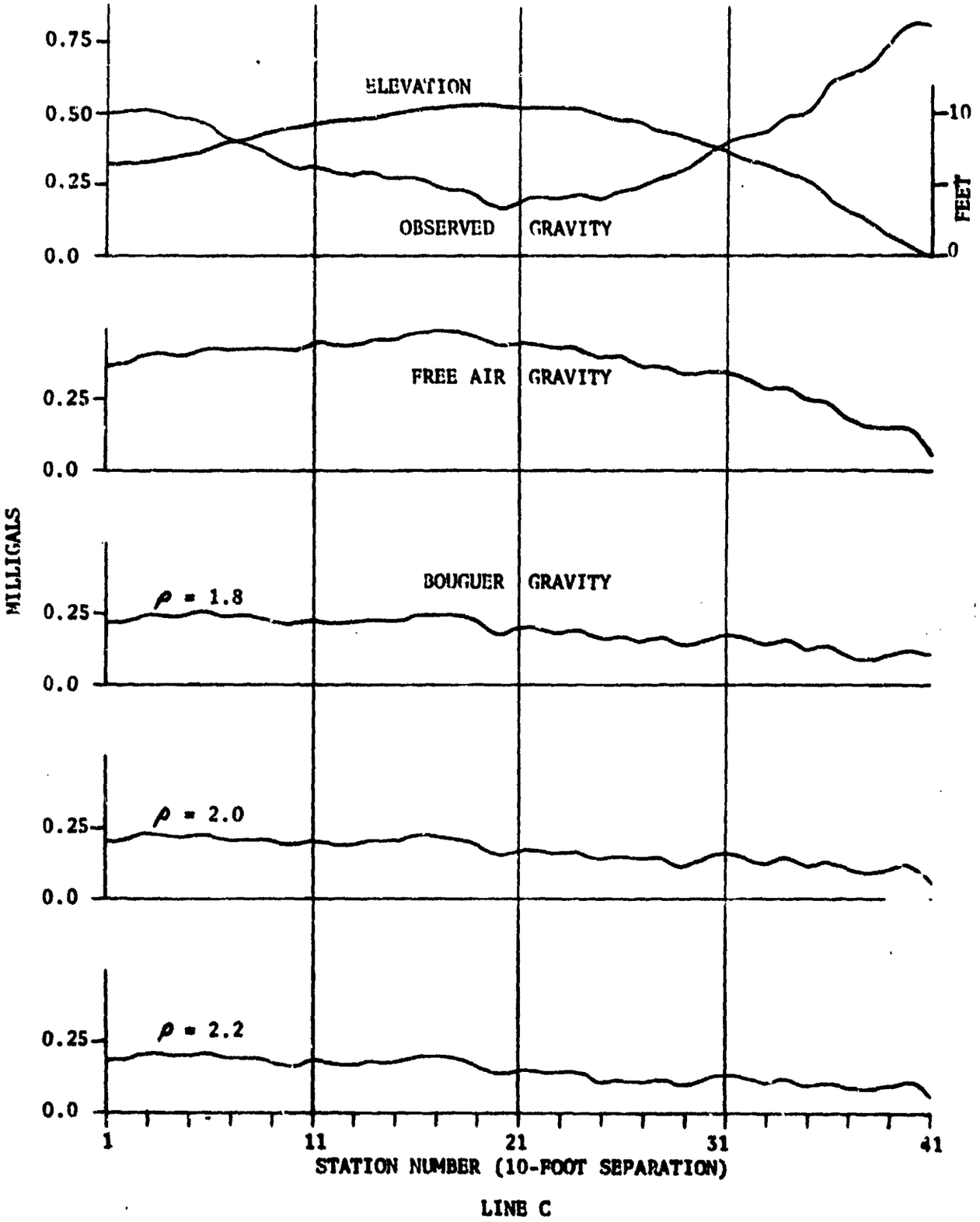

Figure 11. Gravity profile over Traverse T1.

The data from Traverse T3 answers this question. This data is presented in Figure 12. In reference to this figure a duplicate of the results of Watkins et al is seen. This profile was taken over an area suspected of cavities, and upon the attainment of this result a hole was drilled at Station 13. The drill penetrated 15 feet of rock before sinking 120 feet into cave mud before drilling was terminated. A solid bottom was not encountered.

Gravity and electrical resistivity profiles were obtained over this profile and are presented in Figure 13. The position of the drill hole is indicated at Gravity Station 34. This area is both a gravity and electrical resistivity low, well indicative of mud. Parallel resistivity profiles were conducted in an effort to determine if a fault plane or a vertical filled solution cavity had been encountered. The pattern of measurements is shown in Figure 14, and the results are shown in Figures 15 and 16. These results show the circular nature of the mud fill, which points to a cylindrical solution cavity.

From the results of Traverse T3 one questions if the cavity studied by Watkins et al from which they obtained the data of Figure 1 was indeed empty as they claim. The data from T3 is almost identical to theirs. From this result it appears resonable to assume that if strong reverberations are recorded, such as those exhibited by Figure 10 for Traverse T2, that a mud or water filled void has been encountered. This is the only case for which "resonance" is physically plausible anyway.

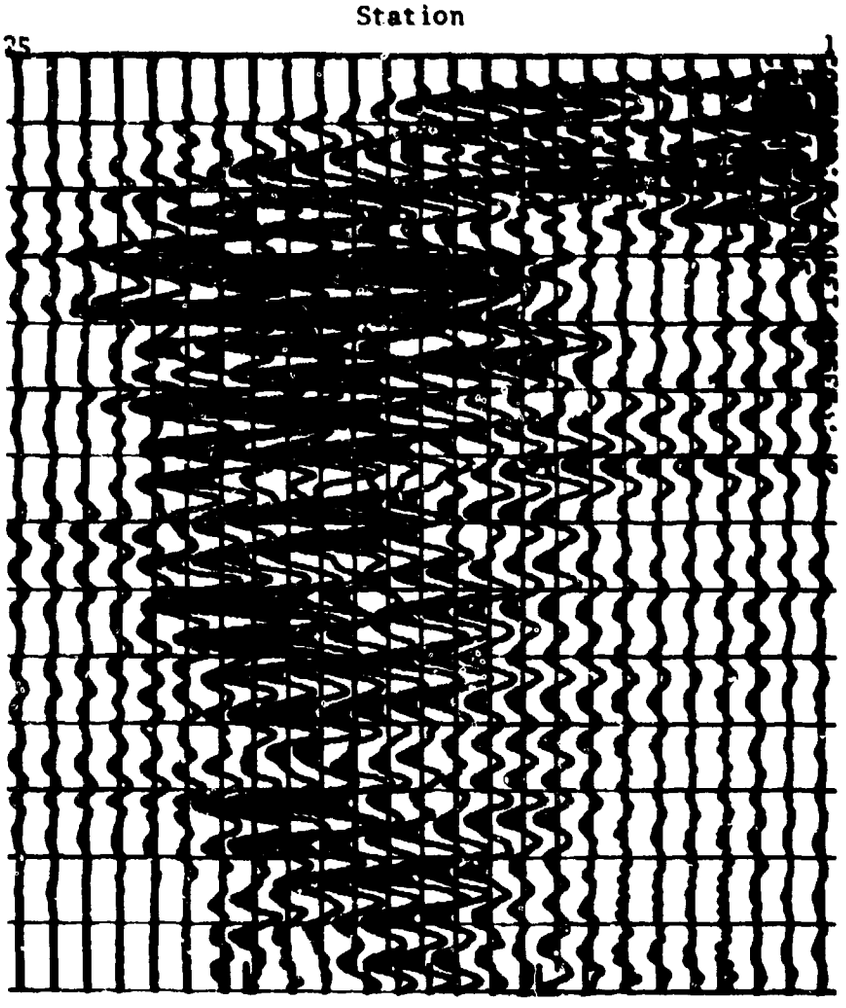

Figure 12. Seismic data over Traverse T3. Spacing 10 foot intervals. Timing interval 100 ms. Shot point 50 feet from end of line at Station 1.

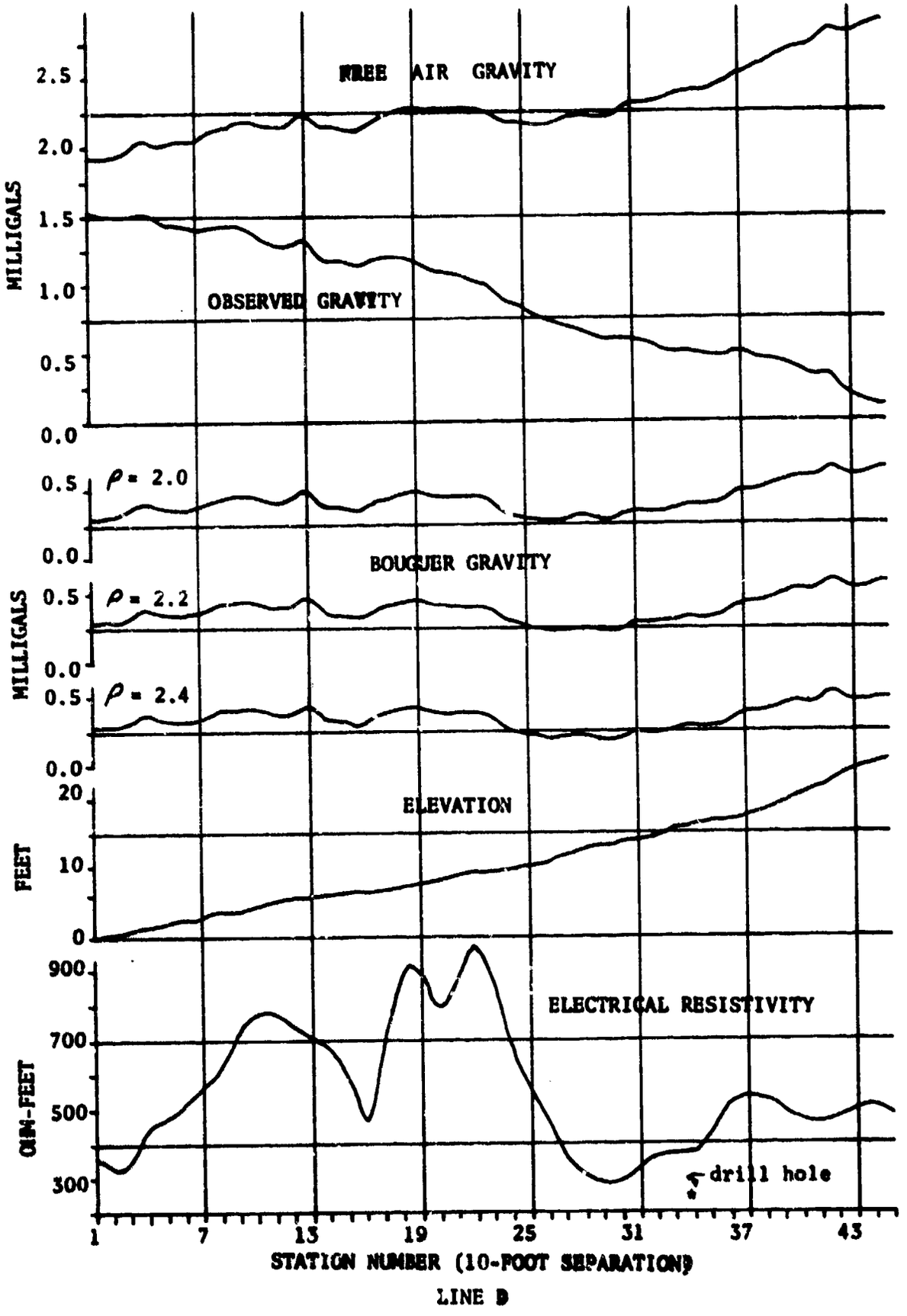

Figure 13. Gravity and Electrical Resistivity profiles for Traverse T3.

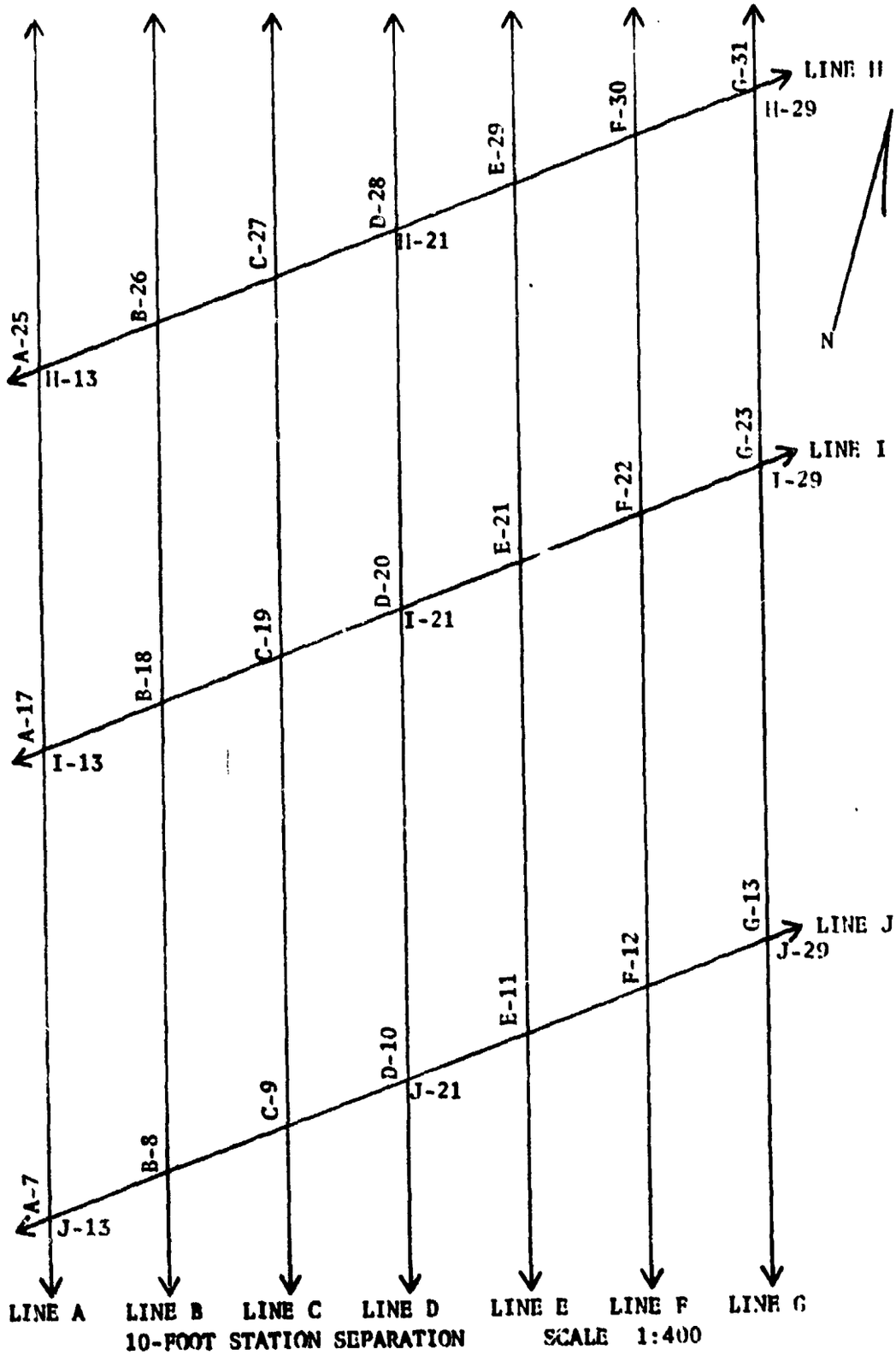

PLAN VIEW OF GRAVITY AND RESISTIVITY TRAVERSE INTERSECTIONS - LOST CAVE RIDGE

Figure 14. Plan view of Electrical Resistivity mapping.

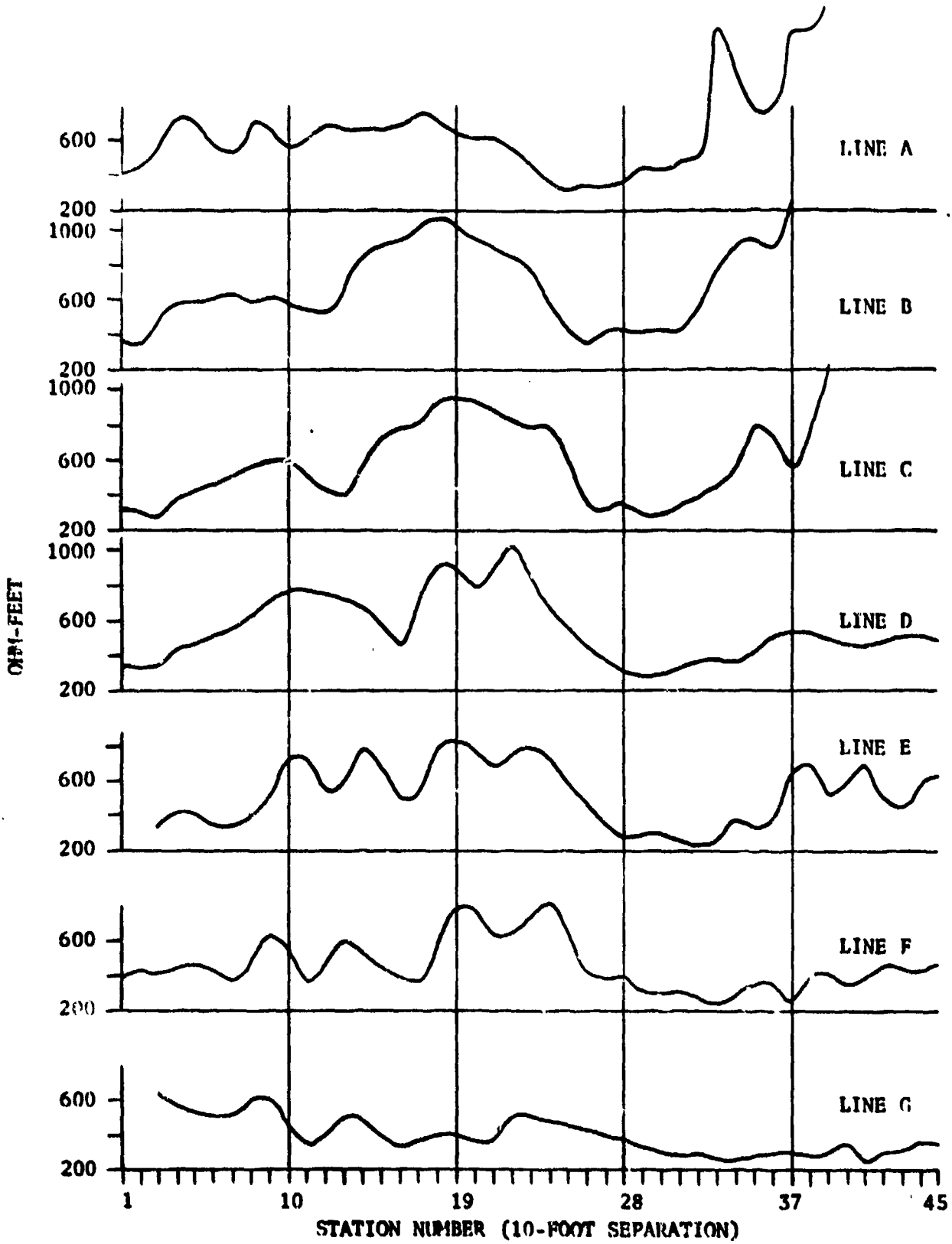

ELECTRICAL RESISTIVITY
LINES A, B, C, D, E, F, G - LOST CAVE RIDGE

Figure 15. North-south Electrical Resistivity profiles.

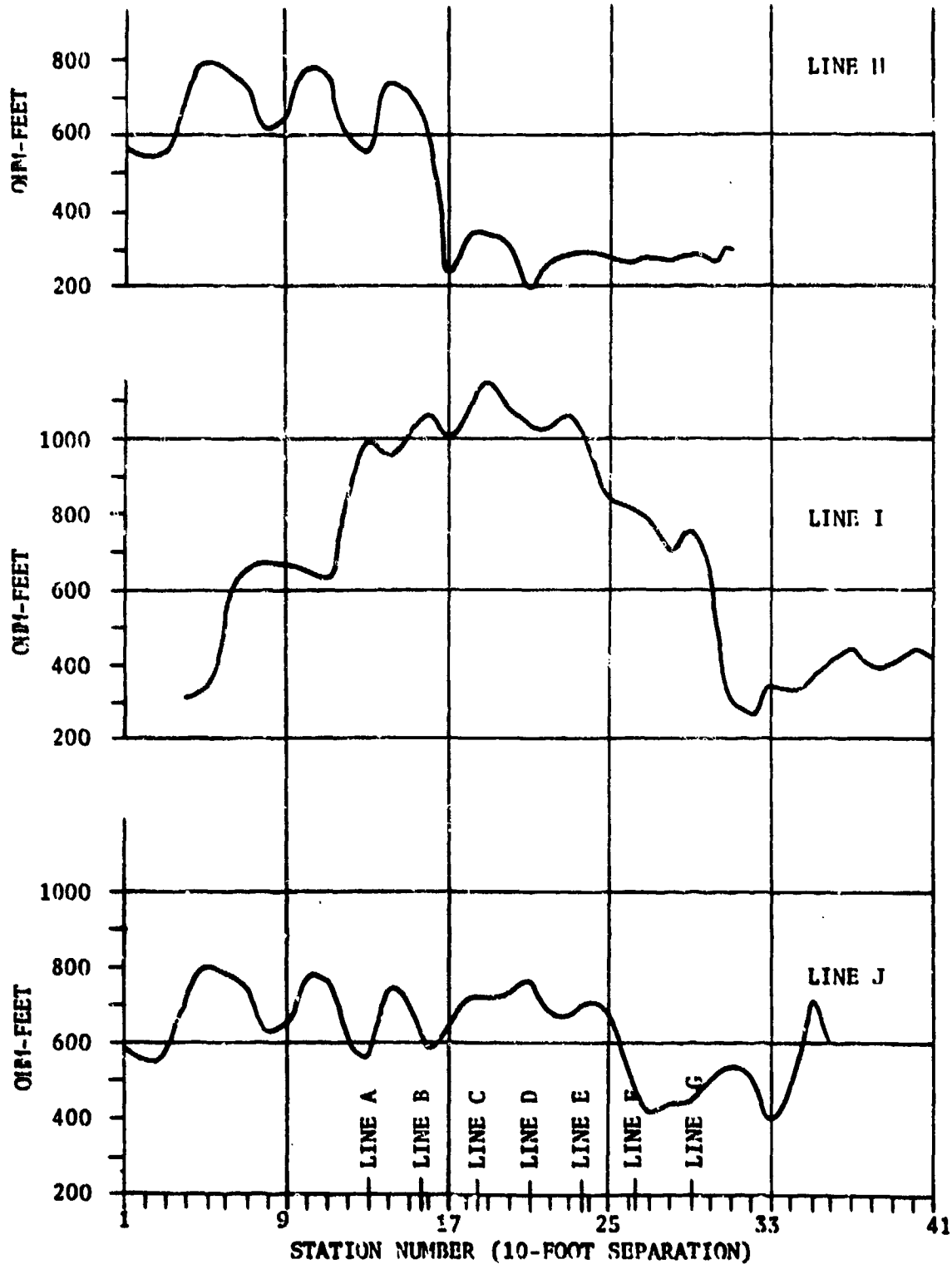

ELECTRICAL RESISTIVITY
LINES II, I, J - LOST CAVE RIDGE

Figure 16. East-west Electrical Resistivity profiles.

CONCLUSIONS

The data presented show two very clear cut examples of cavity signatures in seismic data; one associated with a void cavity, and one for a cavity filled with mud. These signatures, moreover, have been observed on other traverses, over known or suspected cavity areas where the presence of cavities have subsequently been verified by subsurface tunnel exploration or through gravity measurements.

The seismic manifestation of a cavity on a seismogram appears to be the result of the interference of the cavity with passing surface waves. It can be observed in the data that the early Rayleigh and love waves associated with shallow layers that overlie the cavity propagate relatively undisturbed. The deeper penetrating, later arriving surface wave energy, on the other hand, very clearly exhibits the interference effect of the void. The very low frequency of the seismic events manifesting the cavity also point to surface wave energy. Moreover, the abruptness of the lateral variations of the data imply that the seismogram is reflecting the very near surface velocity and density variations, as opposed to the deeper structural variations.

It was initially believed that the cavity signature was a result of the interference of the void with a reflected wave returning to the surface from the basement complex, which for this area is less than 3,000 feet in depth. With an assumed average section velocity of as low as 6,000 feet per second the reflected events would have to occur at record times of less than one second. However, the

velocity is probably higher than 6,000 feet per second and it's hard to account for the later events on the record in terms of reflected wave interference. Moreover, from such a deep reflector, relative to the spread length of the seismic line used in this study, the north and south shots should show a similarity of the reflected events as they are distorted in passing through shallow velocity irregularities. The ray paths would ever be near vertical.

The dissimilarity of the records, the low frequency of the cavity signature, and the very abrupt lateral variations of the events all but negate the plausibility of a reflected wave phenomenon. The surface wave interference theory seems much more reasonable.

The data show that cavities as small as 10 feet in height, 51 feet in width, and 162 feet below the surface can be detected seismically. However, the corresponding seismic signature is not all that obvious in a record section. For example, a very complete set of seismic data obtained with broadside shooting using common depth point coverage, 12 fold, was acquired along a traverse 100 feet from, and paralleling, Traverse T1. But the data was not presented in this report because the data did not show any obvious indication of the cavity which is known to exist beneath this traverse. Only one record, which is presented in Figure 7 of this report, showed the presence of the cavity, but it also didnot exhibit the typical cavity signature. This record was from a shot furthest removed from the line, and represented the most in-line configuration.

This result suggests that two criteria are important in acquiring

seismic data over cavities. First, the shot point and receivers must be in-line. Secondly, perhaps the seismic line must lie at a right angle to the horizontal cavity axis. The first criterion can readily be met in the field. The second is impossible to achieve in unexplored areas.

Cavity detection by seismic means is possible. Yet the procedure is tedious. The required close spacing of the seismometer stations prohibits its use as a reconnaissance tool. The method could be applied effectively over small areas, for instance a dam site, lagoon site, or the like. But the volume of data required for large areas would be prohibitive.

BIBLIOGRAPHY

Biot, M.A., 1952, Propagation of elastic waves in a cylindrical bore containing a fluid: Jour. Appl. Phys., Vol. 23, No. 9, p. 997-1005.

Butkov, E., 1968, Mathematical physics" Reading, Addison-Wesley Co..

Cavanaugh, T., 1975, Three-dimensional ray tracing through heterogeneous media: M.S. Thesis, University of North Carolina at Chapel Hill.

Cavanaugh, T., Stewart, D.M., and Rechtien, R.D., 1975, Mathematical models for anomalous data in the vicinity of caves: 45th Ann. Internat. Mtg., Abs. Soc. Explor. Geophysics, p. 58-59.

Churchill, R.V., 1963, Fourier series and boundary value problems: New York, McGraw-Hill Book Co..

Claerbout, J.F., 1970, Coarse grid calculations of waves in inhomogeneous media with application to delineation of complicated seismic structure: Geophysics, Vol. 35, No. 3, p. 407-418.

Clark, S.P., 1966, Handbook of physical constants: New York, Geol. Soc. Am.

Cook, J.C., 1965, Sesimic mapping of underground cavities using reflection amplitudes: Geophysics, Vol. 30, No. 4, p. 527-538.

Eringer, A.C., 1967, Mechanics of Continua: New York, Wiley Book Co.

Ewing, W.M., 1957, Elastic waves in layered media: New York, McGraw-Hill Book Co..

Godson, R.H. and Watson, J.S., 1968, Seismic resonance investigation of a near-surface cavity in Anchor Reservoir, Wyoming: Bull. Assoc. Eng. Geol., Vol. 5, No. 1, p. 27-36.

Kelly, K.R., Ward, R.W., Treitel, S., and Alford, R.M., 1976, Synthetic seismograms: a finite-difference approach: Geophysics, Vol. 41, No. 1, p. 2-27.

Kolsky, H., 1963, Stress waves in solids: New York, Dover Pubs., Inc..

Landau, L.D. and Lifshitz, E.M., 1959, Theory of elasticity: Addison-Wesley Publishing Co., Inc..

McLachlan, N.W., 1951, Theory of vibrations: New York, Dover Pubs., Inc..

McLachlan, N.W., 1955, Bessel functions for engineers: London, Oxford Univ. Press.

Morse, P.M. and Feshbach, H., 1953, Methods of theoretical physics: New York, McGraw-Hill Book Co..

Rechtien, R.D. and Stewart, D.M., 1975, A seismic investigation over a near-surface cavern: Geoexploration, Vol. 13, p. 235-246.

Richter, C.F., 1958, Elementary seismology: San Francisco, W.H. Freeman and Co..

Stewart, D.M., 1971, The vibrational modes of spherical cavities in elastic solids: Ph.D. Dissertation, University of Missouri-Rolla.

Stilke, G., 1959, On elastic surface waves at a cylindrical hole in an infinite solid: Geophys. Prosp., Vol. 7, No. 3, p. 273-283.

Stravroudis, O.N., 1972, The optics of rays, wave fronts, and caustics: New York, Academic Press.

Watkins, J.S., Godson, R.H., and Watson, K., 1967, Seismic detection of near-surface cavities: Geol. Survey Prof. Paper 599-A.

White, R.M., 1958, Elastic wave scatter at a cylindrical discontinuity in a solid: Jour. Acoustical Soc. Am., Vol. 30, No. 8, p. 771-785.

Ying, C.F. and Truell, R., 1956, Scattering of a plane longitudinal wave by a spherical obstacle in an isotropically elastic solid: Jour. Appl. Phys., Vol. 27, No. 9, p. 1086-1097.

APPENDIX A
Proc. 9th Annual IEEE Computer Society International Conference
September 1974, pp. 249-252

MINICOMPUTERS IN THE ACQUISITION AND ANALYSIS OF SEISMIC DATA

J. H. Tracey, R. D. Rechtien and K. L. Hambacker
University of Missouri-Rolla
Rolla, Missouri 65401

INTRODUCTION

This paper describes the use of a mobile laboratory and minicomputer systems to support geophysics research and instruction at the University of Missouri-Rolla. The equipment includes a mobile van, a field data acquisition system and a minicomputer network for data analysis and classroom replay.

SEISMIC STUDIES

Generalized Seismic Process

Seismic methods are employed to probe the internal stratification of the earth in an effort, generally, to detect and isolate abnormal, localized, geological structures that may exist near the surface[1]. Such structures might be fault zones, solution cavities, salt domes, buried stream channels, or perhaps simply undulations in the rock layers which might be favorable to the accumulation of oil or mineral deposits. Engineering problems, such as the response of tall buildings or dams, to seismic energy, also fall within the broader scope of seismology. Thus, seismic methods deal with the transmission of elastic waves through the heterogeneous earth and, occasionally, their effects on man-made structures.

For the application of seismic methods to non-conventional subsurface problems, it is essential that the experimental test procedures be continually modified upon the acquisition of new information, in order to accomplish a given research task. The researcher must have the flexibility to zero-in on the localized area of interest, and thus avoid the tremendous volume of data required for blind wider-range ground coverage. This flexibility requires that a decision making capability be made an integral part of the test, and as such requires an immediate data analysis capability upon acquisition. The needed system capabilities for near-surface exploration are: the hodograph, or particle trajectory plots, used primarily for wave type identification; the Fast Fourier Transform, used principally for spectral analysis, band-pass filtering, notch filtering, or spectral shaping; cross-correlation; deconvolution; and optimum filtering, used for shaping the frequency spectrum according to some knowledge of prior filtering actions or according to some assumptions about signal characteristics or desired output. These features provide a wide range of field analysis capability.

DESCRIPTION OF MOBILE LABORATORY

The mobile laboratory consists of a converted 2 1/2 ton U.S. Army truck with a completely enclosed rear compartment. The van houses the minicomputer, its peripherals, and associated test equipment. The van is completely air conditioned and capable of being powered from a 220-volt utility outlet or from an on-board generator.

The minicomputer is a NOVA 800 Jumbo Computer with 16K core, and hardware multiply and divide option. A moving head Diablo cartridge disk system with 1.2 million, 16-bit word capacity and a Tektronix 4010 storage-tube graphics terminal are peripheral to the NOVA. A high-speed reader is included for initial loading of application software and utility routines. The system includes an analog-to-digital converter which is capable of converting up to eight analog channels at a maximum rate of 30 KHz for a single channel.

A Texas Instruments DSF (Digital Field System) data recorder is also available in the van. This unit permits the digitization of up to 32 analog channels which can later be played back into the NOVA. The DFS unit is used as a back-up system for the NOVA and is also used in those experiments requiring the continuous digitization of more than eight channels.

FIELD DATA ACQUISITION AND ANALYSIS SYSTEM

Software Development

The software written for the minicomputer[2]

was designed to meet a number of system constraints in terms of program size, speed of execution, ease of operation and invulnerability to user error as well as safety of stored data. The program is completely core resident along with a copy of the Data General Corporation Real Time Operating System for a total length of under 8K words of memory. This leaves 8K words of core for data storage, a transform array, disk I/O buffer, and command sequence storage. Speed of execution received high priority in the software design to minimize user annoyance. This goal of instantaneous machine response is a major factor in keeping the entire program core resident. The command structure is designed to minimize keyboard entries for maximum user time efficiency at the cost of a longer user familiarization period. Single letter mnemonics are used to initially branch to the various areas of program control with all further information being prompted. Considerable effort has been expended to make the system and data resistant to user errors by keying sensitive system parameters which control buffer placement and disk write pointers. As long as this software key is not used the user may randomly type at the keyboard without damaging the program or stored disk data. A break key is defined which allows any operation to be interrupted with a single keystroke. Since considerable time and cost is involved in obtaining data, reliable storage is imperative. For this reason data is stored with distributed identification information so that damage to a critical index sector cannot cause the loss of a major portion of the disk information. The limited amount of code devoted to disk I/O also lowers the chances of a malfunctioning program or machine getting stuck in a loop which damages stored data on disk.

System Operation

Bursts of data from up to eight channels are obtained from the A/D converter at accurately timed rates of up to 1 KHz and stored in core memory. After sampling, a copy of the raw data is immediately stored on disk while the data in core may be manipulated for analysis. Individual channels of data may have a DC level removed, be shifted in time, and be normalized in amplitude. Channels may be added, subtracted, and multiplied collectively for such operations as signal averaging. Arrays of time samples may be normalized and Fast Fourier Transformed at 2^{10} samples in about one and one half seconds. The spectrum may be modified and an inverse transform obtained. Also, single events of interest in a waveform may be isolated or used as models for wavelets entered from a digitizing tablet.

A2

A variety of displays are available of the data or functions of the data without any modification to the data arrays used or storage of the resultant functions. All plots may be scaled by powers of two and offset to display any desired window of information. Vertical and horizontal markers are scaled to be consistent with the displays for waveform measurement. Thousand-point plots typically take slightly over two seconds. Single channel time plots are available of information stored in the sample buffer and of real information stored in the transform array. If the information in the transform array is rectangular complex spectral information, magnitude and phase angle functions may be plotted as well as the stored real and imaginary representations of the transform. Several plots involving more than one channel of sampled information are available. Windowed plots of particle position with time may be derived from three channels of data. Oblique and projected views from any angle are allowed at selectable speeds up to maximum terminal plotting speed. Particle plots may be interrupted for point number identification and then continued to allow isolation of individual events in the three dimensional representation. Displays are also available of correlation and convolution functions of any two channels of sample data.

The command structure of the program allows rapid and convenient use of various analysis methods and hence allows the user to concentrate on innovative techniques for data reduction which might be neglected or missed in a system with slower turnaround. Once a promising sequence of analysis steps has been arrived at it may be stored and recalled at

will for use on other data sets. This feature of the program has proved indispensable for the orderly display and analysis of three-axis data where the same operations are required for each channel. The command sequences are not intended for use in building basic new functions, which are best implemented in assembler code, but means are available to enter run time variables, do simple arithmetic, do an arithmetic branch, pause for displays and set up loops. These command sequences are stored and executed as they are initially entered, so errors are detected immediately and preparation time is kept to that normally required for command keyboard entry.

ROLE OF UMR COMPUTER NETWORK

Figure 1 shows a portion of the current configuration of the UMR minicomputer network[3] which complements the data acquisition system described in the previous sections. The network consists of a NOVA minicomputer co-located with and attached to the multiplexor channel of an IBM 360/50 Computer. Several remote minicomputers are attached via high-speed lines (50K baud) to this front-end processor. The front-end processor communicates directly with the 360/50 through its I/O channel, controls the high-speed communication lines, and controls several low-speed devices such as a paper tape reader, and punch and mark sense card reader. Other devices, peripheral to the 360/50, are controlled by the remote minicomputers. The total system permits a wide variety of I/O devices which in turn can handle data in many different forms. Data can be input to the system from paper tape, analog signals, line drawings (traced on a graphics table), pictures (constructed on a graphics terminal), or removable disk cartridges.

When the mobile van is outfitted for field experimentation, one of the Computer Center NOVA's (see Figure 1) is removed and installed in the van. In the field, two seismometers are placed in appropriate positions and the ground is set in motion with either an explosive charge or a shaker. Each seismometer supplies three analog signals, one for each component of displacement. These six analog signals are digitized for the duration of the experiment and the data is transferred to disk. The data can be previewed in the field and relatively small records (~ 1000 pts. per channel) can be analyzed as described in the previous section. This cursory analysis is very beneficial for data verification and on-site determination of future seismometer and disturbance placement.

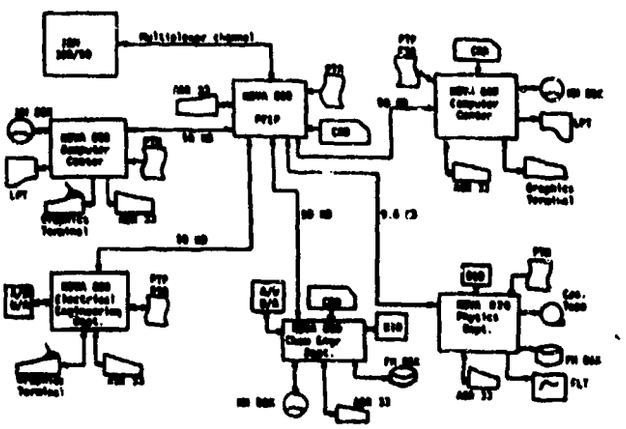

Figure 1. Partial Arrangement of UMR Minicomputer Network.

The disk cartridge which contains the field data can be removed from the mobile van NOVA and loaded in a second NOVA located in the Computer Center and networked to the IBM 360/50. There, the data is transferred to the 360/50 disk. At this point, the experimenter can perform more sophisticated analysis of the data and make use of the higher performance peripherals. At present, the 360/50 is used to plot the data and calculation results on a Calcomp plotter and punch some of the shorter records on cards for permanent storage. Longer data records will be stored on magnetic tape. In addition, correlations and transforms can be conveniently calculated for much larger data sets than can be processed in the minicomputer. A future project will involve a pattern recognition and feature extraction program which will run on the 360/50 to assist the experimenter in his visual analysis of data and calculated results.

The total system permits real-time field data acquisition, analysis, and quick-look followed by central computer analysis with permanent records in the form of plots, cards, disk and tape storage.

INSTRUCTIONAL BENEFITS

The entire data acquisition system can be dismantled, reinstalled in either the computer center or the mobile van, and be in operation within a period of five hours. Consequently, there is considerable flexibility in using the instrument as an acquisition system in the field, or as an instructional and research instrument in the laboratory. During the academic year the system is normally used for instruction and processing of field data acquired during the summer.

The system is extremely unique in providing a training facility for geophysics students. By use of this instrument, these students can acquire a thorough familiarity with elastic wave methods through study of wave forms, particle motion, correlation theory, numerical filtering, and deconvolution by manipulation of real data with an immediate visual result of the operations. Many variations of the filter parameters, for example, can be obtained in a very short period of time, thus giving the student a very sound feeling of each process. Further, the student is only required to obtain a very superficial knowledge of the computer programs, and no programming as such is necessary.

SUMMARY

The paper describes the application of minicomputers to the research and instructional areas of geophysics. The system described here uses a minicomputer in a mobile van for the acquisition and preliminary field analysis of data produced in generalized seismic experiments. The minicomputer controls the acquisition, storage and display of raw data and transformed data. The data is then manually transferred to a separate but similar minicomputer for loading into a larger computing system for further analysis and storage. Lastly, the data may be retrieved and displayed for classroom use as a partial substitute for actual field experimentation.

REFERENCES

1. R. D. Rechtien and D. M. Stewart, "A Seismic Investigation Over a Near-Surface Cavern", accepted for publication, Geoexploration.
2. K. L. Hambacker, "SPECTRUM - Interactive Data Acquisition and Analysis Program for NOVA Computer", Technical Report, CRL 74.3, (August, 1974).
3. H. J. Pottinger, "Considerations in the Design of a Network of Minicomputers", Ph.D. Dissertation, University of Missouri-Rolla, Rolla, Missouri (1973).